THE UNIVERSITY OF NEW MEXICO
HEALTH SCIENCES CENTER
COLLEGE OF PHARMACY
ALBUQUERQUE, NEW MEXICO

Correspondence Continuing Education Courses
for Nuclear Pharmacists and Nuclear
Medicine Professionals

VOLUME 10, NUMBER 5

Advances in PET Imaging

By

Mark T. Madsen, PhD, FAAPM, FACR
Professor of Radiology
University of Iowa

The University of New Mexico Health Sciences Center College of Pharmacy is accredited by the American Council on Pharmaceutical Education as a provider of continuing pharmaceutical education. Program No. 039-000-02-005-H04. 3.5 Contact Hours of .35 CEUs. Expires 08/01/2005.

Advances in PET Imaging

By:

Mark T. Madsen, PhD, FAAPM, FACR

ADVANCES IN PET IMAGING

STATEMENT OF OBJECTIVES

Upon completion of this lesson, the reader should be able to:

1. Identify the advantages PET tracers and instrumentation have over conventional Nuclear Medicine and other imaging modalities.

2. Understand how the fundamentals of positron decay, annihilation radiation and coincidence detection provide PET with superior imaging capabilities.

3. Understand the design of dedicated PET imaging systems and SPECT/PET imaging systems.

4. Identify the required corrections for PET imaging and their impact on image quality.

5. Understand the fundamentals of PET image reconstruction.

6. Compare the advantages of 2D and 3D PET imaging.

7. Understand the role of combined PET and CT imaging systems.

8. Understand the design of small animal PET imaging systems.

COURSE OUTLINE

THE MOTIVATION FOR PET

A. Radiotracers

B. Reimbursement

C. Coincidence Detection

II. PET FUNDAMENTALS

A. Positron Emission (Figure 1)

B. Annihilation Radiation (Figure 2)

C. Production of Positron Emitters

D. Annihilation Photon Interactions

D.1 Photoelectric Absorption (Figure 3)

D.2 Compton Scatter (Figure 4)

E. Detector Efficiency

E.1 Geometric Efficiency

E.2 Intrinsic Efficiency

F. Singles detection (Figure 5)

G. Coincidence Detection (Figure 6)

G.1 Coincidence Efficiency

G.2 Coincidence Simultaneity

G.3 Random Coincidences (Figure 7)

G.4 Scattered Radiation (Figure 8)

III. PET SCANNER DESIGN

A. Ring Detectors

B. Scintillators

B.1 Materials

B.2 Photomultiplier Tube Sharing

C. PET Systems

D. HRRT (High Resolution Research Tomograph)

E. PET Spatial Resolution

E.1 Detector Face Size

E.2 Detector Thickness

E.3 Ring Diameter

E.4 Data Smoothing

E.5 Pixel Size

E.6 Positron Range

F. SPECT/PET Systems

G. SPECT/PET Challenges

H. C-PET

IV. PET CORRECTIONS

A. Sensitivity

B. Random Coincidences

C. Scattered Radiation

C. Attenuation Correction

C.1 Attenuation Artifacts

C.2 Transmission Scans

C.3 Transmission Noise

V. PET RECONSTRUCTION ALGORITHMS

A. Sinograms

B. Backprojection

C. Filtered Backprojection

D. Iterative Algortithms

E. Ordered Subsets

F. 3D PET Reconstruction

F.1 Fourier Rebinning

F.2 RAMLA

F.3 MAP Routines

VI. 2D vs. 3D PET

A. 2D PET Design

B. 3D PET Design

B.1 3D Sensitivity

B.2 Noise Equivalent Count Rate

VII. PET/CT

A. PET Systems

B. Combined PET and CT Systems

C. Co-registration

D. PET/CT Disadavantages

E. PET/CT Artifacts

E.1 CT Field of View Truncation

E.2 Breathing Artifacts

E.3 Contrast Artifacts

E.4 Metal Artifacts

VIII. SMALL ANIMAL PET SYSTEMS

A. Estimated Scanner Requirements

B. Other Challenges

C. Design of Small Animal PET Systems

ADVANCES IN PET IMAGING

By
Mark T. Madsen, PhD, FAAPM, FACR
Professor of Radiology
University of Iowa

THE MOTIVATION FOR PET

Although positron emission tomography (PET) has been available for more than 20 years, it was not widely used until about 5 years ago. Instead of being an elite tool of a handful of academic institutions, it is now available throughout the country even in rural communities. PET images are distinctly noisier and inferior in spatial resolution compared with computed tomography (CT) or magnetic resonance imaging (MRI). However, the power of PET resides in its ability to capture physiology and thereby obtain crucial diagnostic information unavailable from high-resolution pictures of the anatomy. The recent explosion of interest in positron emission tomography (PET) as a diagnostic imaging modality originates from three factors: powerful radiotracers, coincidence detection, and study reimbursement.

A. Radiotracers

The first factor comes from the advantages positron-emitting radionuclides offer as radiotracers. Radionuclides that emit high-energy photons are nearly ideal tracers for biological systems. One reason for this is that the penetrating nature of the photons (x-rays, gamma rays or annihilation radiation) allows them to be non-invasively monitored with external detectors. Another big advantage is that the amount of material required for detection is incredibly small. Typically, the amount of administered activity corresponds to less than 10 nanograms of material. At these levels, there is little chance of perturbing the physiological state of the tissues and organs and there is virtually no toxicity. This gives the radiotracer approach a sensitivity that is unmatched by any other diagnostic modality. In addition to the advantages associated with radionuclides, there are positron-emitting radioisotopes of carbon, nitrogen, oxygen, and fluorine. These elements can chemically combine with a virtually unlimited number of vital and diagnostically interesting molecules. While there are a few gamma-emitting radioisotopes for some of these elements, they have neither the appropriate energy nor the appropriate half-life to make them useful radiotracers for diagnostic imaging studies. The list of radiotracers that have been labeled with positron emitting radionuclides is in the hundreds and grows longer with each year. This list includes positron-emitting radiotracers for blood flow, glucose metabolism, hypoxia, monoclonal antibodies, gene expression, amino acid metabolism and a wide variety of receptors and transporter agents. The most versatile clinical PET radiopharmaceutical is F-18 Fluoro-2-deoxyglucose (F-18 FDG) a glucose analog. F-18 FDG is accumulated in high concentration in metabolically active tumors as well as in brain and the myocardium. Although the half-life of F-18 is only 110 minutes, F-18 FDG is available throughout the U.S. in unit dose quantities. Other PET radiopharmaceuticals with potentially high clinical impact are deoxy-[F-18]fluorothymidine (FLT) for tumor imaging, F-18 fluorocholine for prostate cancer, F-18 fluoradopa for brain receptor imaging, and N-13 ammonia for myocardial perfusion imagng.[1-14]

B. Reimbursement

The second factor for the growth of PET is that the Centers for Medical & Medicaid Services (CMS) is reimbursing PET studies for a significant number of indications. These include the use of F-18 FDG in the diagnosis, staging and restaging of non-small cell lung cancer, esophageal cancer, colorectal cancer, head and neck cancers, lymphoma and melanoma, as well as the staging and restaging of breast cancer. It also includes coverage for myocardial viability and the pre-surgical evaluation of refractory seizures with F-18 FDG and myocardial perfusion with Rb-82 and N-13 ammonia. Combined, these categories encompass a large patient population. As a result, medical facilities across the nation have begun including PET as part of their diagnostic services.[15]

C. Coincidence Detection

The third factor is the unsurpassed spatial resolution and count sensitivity PET offers relative to conventional nuclear medicine imaging. PET spatial resolution is about 100% better than that obtained with single photon emission computed tomography (SPECT) and the count sensitivity is approximately 20–30 times higher. PET achieves these gains from the coincidence detection made possible by the nature of the annihilation photons resulting from positron emission.[16-19]

II. PET FUNDAMENTALS

A. Positron Emission (Figure 1)

There is a class of radioactive materials that decay by turning one of the protons within the nucleus into a neutron. As part of this radioactive decay process, an energetic positron is created and emitted from the nucleus. These radionuclides are called positron emitters. The positron is the antiparticle of the electron. It has the same size and mass as an electron, but its charge is positive. Positrons are emitted with energies that range from zero up to the total available energy from the decay. This is because the energy associated with the transformation is split between the positron and a neutrino that is also created at the instant of decay.

Figure 1. Positron Decay. With positron decay, a proton in the nucleus is converted to a neutron with the emission of a positron and a neutrino.

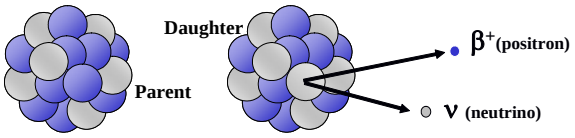

B. Annihilation Radiation (Figure 2)

Positrons lose energy as they traverse through tissue by ionizing and exciting bound electrons. As the positron reaches the end of its range, it captures an electron. The particles form a positronium atom where the electron and positron orbit about their common center of mass. Within a microsecond, the two particles completely annihilate each other resulting in two 511 keV photons corresponding to the complete conversion of the electron and positron masses to energy. If the positronium atom is at rest when the annihilation occurs, the two annihilation photons must travel in exactly opposite directions to conserve momentum. However, the thermal vibrations associated with the ambient temperature cause slight deviations such that the angle between the annihilation photons has a variance of ± 0.25 degrees from 180°.

Figure 2. Annihilation Radiation. The mutual annihilation of an electron and its anti-particle, the positron, results in two co-linear 511 keV photons.

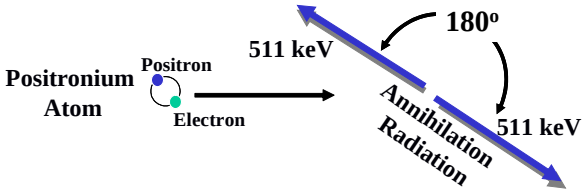

C. Production of Positron Emitters

The production of positron emitting radionuclides requires a charged particle accelerator such as a cyclotron to bombard the target material with protons or deuterons. F-18 is produced by shooting protons at a target with enriched O-18 water:

$$^{18}O + p \rightarrow {}^{18}F + n$$

Positron emitters with short half-lives such as O-15, C-11, and N-13 have to be produced by a local accelerator. F-18 has a long enough half-life that is can be delivered over hundreds of miles. Rb-82 is available from a radionuclide generator with a long shelf life.

D. Annihilation Photon Interactions

It will be useful to review how annihilation photons interact with different materials. From a practical point of view, there are only two interactions that annihilation photons are likely to have, photoelectric absorption and Compton scattering. Photoelectric absorption is the primary interaction in the detectors and shielding while Compton scatter is the primary interaction in body tissue.

D.1 Photoelectric Absorption (Figure 3)

With photoelectric absorption, a high-energy photon is completely absorbed by an inner shell electron and the electron is ejected from the atom. The cross section (likelihood of an interaction) is proportional to $Z^3\rho/E^3$, where Z is the atomic number of the interacting material, ρ its density and E the energy of the photon. Because of the dependence on atomic number and energy, the cross section for photoelectric absorption in body tissues for annihilation radiation is very low. Photoelectric absorption in the detectors is highly desirable and therefore, useful detector materials must have high atomic numbers and density (section III B.1)

Figure 3. Photoelectric Absorption. With photoelectric absorption, a photon is completely absorbed by an inner shell electron. The electron is ejected from the atom, the resulting inner shell vacancy yields characteristic x-rays, and Auger electron as the vacancy is filled.

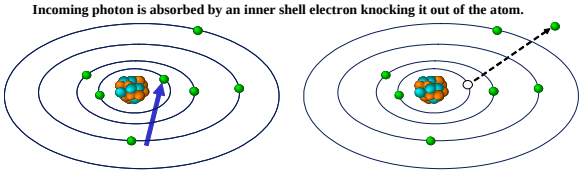

D.2 Compton Scatter (Figure 4)

Compton scatter is the most common interaction inside patients for annihilation radiation. It causes a loss of image contrast and significant efforts are devoted toward removing it from PET images. Unlike photoelectric absorption, the Compton scatter cross section depends primarily on material density and falls slowly with photon energy. With Compton scatter, a high-energy photon has a billiard ball like collision with a loosely bound electron. The photon changes direction and looses energy, with the lost energy being transferred to the scattered electron. The amount of energy loss depends on the scattering angle. The loss of energy is one-way detection systems that have energy resolution can remove scatter by only accepting events that have the full primary photon energy.

Figure 4. Compton Scatter. With Compton scatter, the incoming photon transfers a portion of its energy to an outer shell electron resulting in both an energetic electron and a scattered photon.

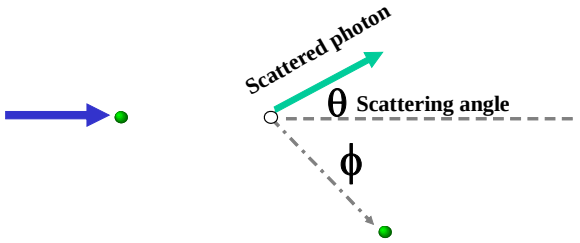

E. Detector Efficiency

E.1 Geometric Efficiency

In the following section, the basics of coincidence detection are discussed and it will be useful to understand the concept of detector efficiency. Detector efficiency refers to the capability of a detector to absorb and register annihilation radiation. Because image quality depends on the number of detected events in the study, detector efficiency is a very important consideration. Detector efficiency has two components. The *geometric efficiency* refers to the fraction of emitted annihilation photons that hit the detectors and that depends on the area of the detectors and the source to detector distance. To maximize geometric efficiency, the detectors should be close to the source (i.e., the patient) and the detector area should encompass the entire patient.

E.2 Intrinsic Efficiency

The other component of detector efficiency is the *intrinsic efficiency*. The intrinsic efficiency is the fraction of those annihilation photons that hit the detector that are detected. It is desirable to have the intrinsic efficiency be as close to 1 (i.e., 100% detection) as possible, and that is especially important for coincidence detection. The intrinsic efficiency of a detector is related to its cross section for photoelectric absorption and that depends strongly on the detector atomic number and density. These features are reflected in the properties of the commonly used PET detectors. The other factor that affects intrinsic efficiency is the detector thickness.

PET scanners are made up of a large array of detectors. The next several sections describe briefly how detection of annihilation radiation is accomplished.

F. Singles detection (Figure 5)

In a conventional detector, a high-energy photon interacts with the detection material and creates an electronic pulse. The energy absorbed in the interaction is reflected by the amplitude of the electronic pulse (the pulse height). For photoelectric absorptions, the pulse height is directly proportional to the photon energy. A pulse height analyzer is used to select the electronic pulses within a certain energy range. Usually the pulse height energy window is centered on the portion of the energy spectrum corresponding to total photon absorption (the photopeak). A logic pulse is generated for each event that falls in the selected energy window and these are counted by a scaler. This arrangement is often called *singles detection* and the recorded events the *singles counts* to distinguish from the coincidence events described below. Spatial resolution with singles detection requires collimation. A collimator is usually made of lead and has a low efficiency. Holes in the lead allow photons to hit the detector from limited locations. At 511 keV, a large amount of lead is required to provide effective collimation and this lead reduces the count sensitivity of the detector.

Figure 5. Singles Detection. Photons that are absorbed in the detector create electronic pulses that contain energy and timing information. Spatial resolution in the singles detection mode requires collimation.

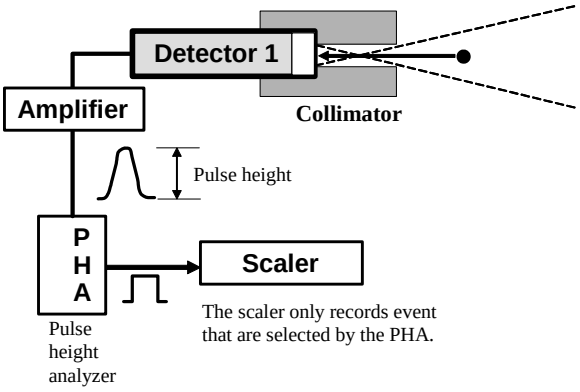

G. Coincidence Detection (Figure 6)

Coincidence detection provides spatial resolution without the need for lead collimation. Coincidence detection takes advantage of the fact that the annihilation photons resulting from positron emission are colinear. Events are counted only if two opposed detectors simultaneously detect them. As illustrated in Figure 6, two single detection systems are used with an additional coincidence module. Each individual system will generate a logic pulse when they detect an event that falls in the selected energy window. If the two logic pulses overlap in time at the coincidence module, a coincidence event is recorded. PET systems use a large number (~10,000) of detectors in coincidence arranged in a ring to collect the projection information required for tomography. The important issues associated with coincidence detection are discussed below.

Figure 6. Coincidence Detection. With coincidence detection, events are counted only if there is simultaneous detection of the annihilation photons at two opposed detectors. Spatial resolution depends on the detector geometry.

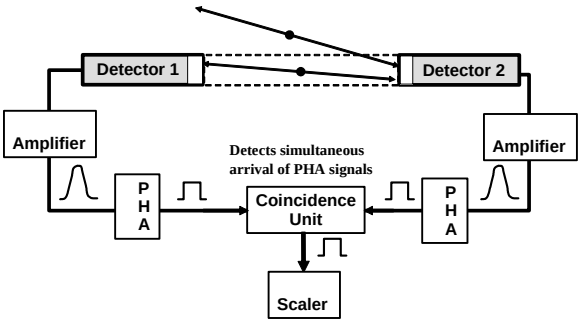

G.1 Coincidence Efficiency

The intrinsic detection efficiency for a singles detector depends on the atomic number, density, and thickness of the detector. Ideally, the intrinsic detection efficiency should be 1, but at 511 keV that is not practical because of the detectors would be too thick. However, intrinsic efficiencies approaching 0.9 can be achieved. Coincidence detection requires that both detectors register an event. Since the interactions at the two detectors are independent events, the coincidence intrinsic efficiency depends on the product of the intrinsic efficiency at each detector. For example, if the intrinsic efficiency of the individual detectors is 0.8, the coincidence efficiency will be $0.8 \times 0.8 = 0.64$.

G.2 Coincidence Simultaneity

A coincidence event is recorded when there is an overlap of the singles logic outputs at the coincidence modules. The time width of the overlap depends on the scintillation characteristics of the detectors. For current PET scanners, that width ranges from 6–12 nanoseconds (1 nanosecond = 10^{-9} s). Although that is a very short time compared to most human activities, it is a long time when compared to distances cov-

ered by photons traveling at the speed of light. Light travels approximately 30 cm (1 foot) per nanosecond so that even a 6-nanosecond duration corresponds to a length 3 times larger than the scanner diameter. As a result, the differential distance of the source between detectors has no observable effect on the timing of the coincidence events.

G.3 Random Coincidences (Figure 7)

The only criterion for recording a coincidence event is the overlap of output pulses at the coincidence module. As the count rate at each of the singles detectors increases, the chance of this occurring from uncorrelated events increases. These events are called random or accidental coincidences. The random coincidence rate is directly proportional to the width of the coincidence time window and the product of the singles rate at the two detectors. At high count rates, the random coincidence rate can exceed the true coincidence rate. The random coincidences provide false information and need to be removed.

Figure 7. Random Coincidences. The registration of a coincidence event from two uncorrelated sources. Random coincidences must be subtracted from the measured data.

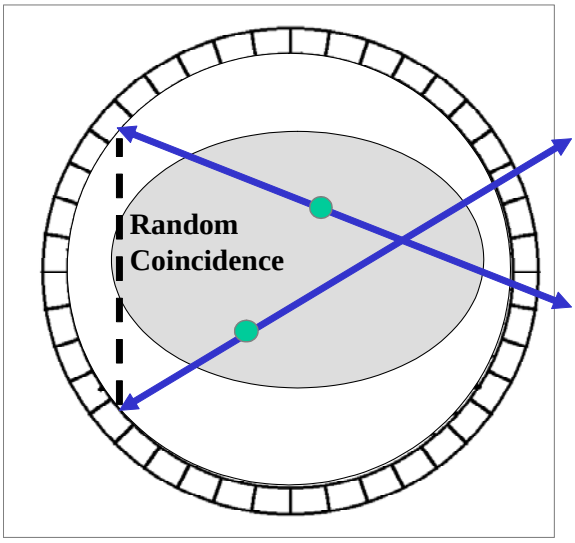

G.4 Scattered Radiation (Figure 8)

For sources in air, it is only possible to get a true coincidence event if the source lies in the defining volume between the two detectors. However, if the sources are in some material like human tissue for example, it is possible for one or both of the annihilation photons to have a Compton interaction to cause a coincidence event. This is undesirable and considerable effort goes into either rejecting scattered events or subtracting them from the acquired data. As discussed above, scattered radiation has a lower energy than the expected 511 keV annihilation radiation and the number of scattered events can be reduced by selecting an energy window centered on 511 keV. However, this does not eliminate it all and additional scatter correction techniques are required for PET imaging.

Figure 8. Scattered Coincidences. If one or more of the annihilation photons is Compton scattered, the resulting coincidence event does not accurately reflect the source location.

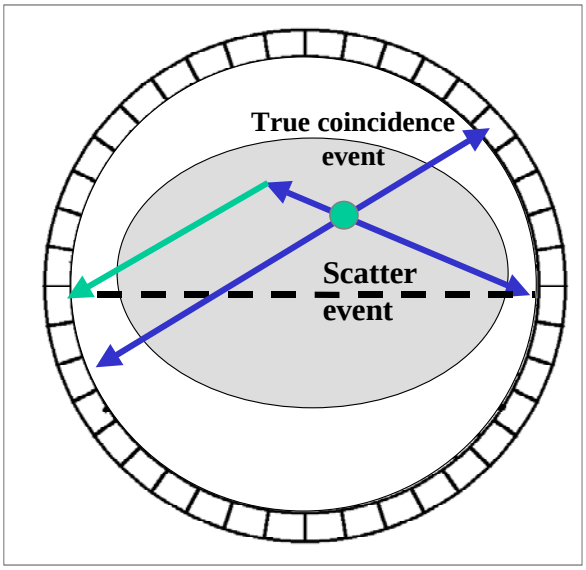

III. PET SCANNER DESIGN

PET imaging systems are based on coincidence detection. In this section, the vari-

ous designs that are currently available will be discussed. This will include a brief description of the PET/SPECT systems and the gamma camera based C-PET system. However, most of the discussion will be focused on the high performance ring detector configurations. Description of the PET/CT systems will be deferred to a subsequent section.

A. Ring Detectors

The best performing whole body PET systems have a large array of detectors that form a cylinder that the patient passes through. If a single ring of this system is considered, each detector within the ring can form a coincidence event with any of the opposing detectors as shown in Figure 9. Each potential coincidence connection is called a *line of response*. These lines of response provide all the necessary sampling to generate a tomographic image for one plane. To increase the number of planes, additional rings are combined together to form a large cylinder covering 16–18 cm. The number of detectors used in commercial whole body PET systems ranges from 9,000–18,000.[16-24]

Figure 9. PET Ring Detector. Most commercial PET scanners have many individual detectors arranged in rings to provide the required data sampling for tomography. Multiple rings stacked together provide the axial field of view.

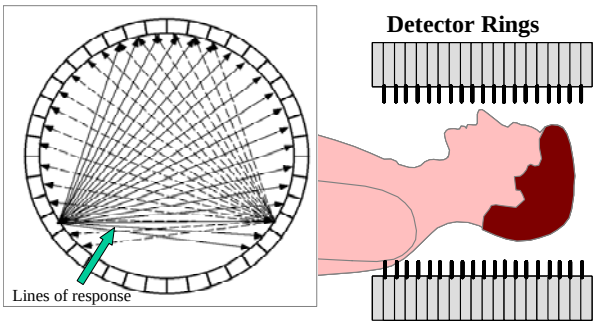

B. Scintillators

As previously discussed, coincidence detection requires high intrinsic efficiency. This means the detectors must have both high density and high atomic number. The materials that best suit these needs are scintillators. Scintillators emit visible light when they absorb radiation. The visible light is then turned into an electronic pulse by a photomultiplier tube. In addition to high intrinsic efficiency, other properties are important for scintillators. These include the intensity and duration of the scintillation. A high light output is desired for good energy resolution. Energy resolution quantifies how well the detector can determine the energy of the detected event and it is useful for discriminating against scattered radiation. Essentially, it is defined as 100% times the uncertainty in the energy/actual energy. Thus, perfect energy resolution is 0% and larger numbers indicate worse performance. Short scintillation duration allows a tighter coincidence window to reduce random coincidences and allows the detector to operate at a high-count rate without losses resulting from "dead time." Dead time refers to the time the system is insensitive to new events because it is processing the current event.[19, 22, 25]

B.1 Materials

Three scintillators are currently being used for whole body PET systems: bismuth germanate (BGO), lutiteum oxyorthosilicate (LSO) and gadolinium oxyorthosilicate (GSO). Their properties are summarized in Table 1. BGO has the best intrinsic efficiency, but its light output is very low and the scintillation decay time is quite long. As would be expected, this results in poor energy resolution and count rate capability. LSO coincidence intrinsic efficiency is 7% below that of BGO, but it has a very high light output and the scintillation decay time is almost a factor of 10 shorter. This makes LSO a very attractive detector. One problem LSO has that the other detectors do not share is that it is actually radioactive. The

detectors have a continual background detection rate. Fortunately, this is not a significant problem in the coincidence mode. GSO intrinsic efficiency is 22% less than BGO, but it also has a much higher light output and short decay time.[16-24]

B.2 Photomultiplier Tube Sharing

As stated above, whole body PET systems can have 9,000 to 18,000 individual detectors. In the early PET scanners, each detector was coupled directly to a single photomultiplier tube (PMT). The size of the photomultiplier tube was at that time the limiting factor to detector size and therefore the limiting factor to PET resolution. In the 1980s, the concept of the detector block was developed (Figure 10). In this scheme, an 8 × 8 array of detectors is coupled to four photomultiplier tubes. Each detector in the array is identified accurately from the ratios of the difference and sums of the photomultiplier tube signals. This innovation was very important since it provided an economical solution to reducing the detector size while preserving count sensitivity. Block detectors are still in use by Siemens and General Electric. The Philips Allegro uses an approach similar to the Anger logic used on a scintillation camera. In their design, an array of photomultiplier tubes views the detector matrix. When an event occurs, the involved detector is determined from summing the position weighted signals of the pmts in the event proximity. Both of these approaches permit the use of very small detectors. In PET whole body systems, the detector face size is approximately 6 × 6 mm (Table 2). For small animal PET systems, the detector face size is approaching 1 × 1 mm.[16-24]

Figure 10. Block Detector Design. Multiple small detectors are arranged in arrays (blocks) that are coupled to 4 photomultiplier tubes. This configuration allows the accurate identification of the detector that absorbed the annihilation photon.

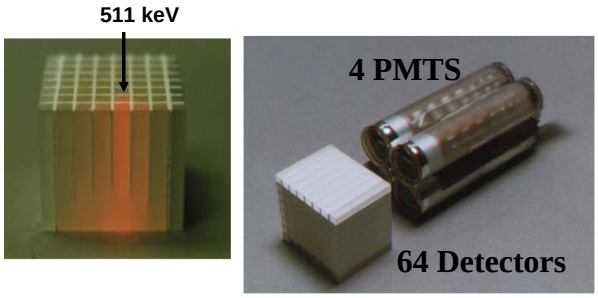

C. PET Systems

Table 2 gives the design parameters for the most commonly used PET whole body systems, the CTI Reveal/Siemens Accel, the CTI Reveal Hi-Rez, the GE Advance Nxi, GE Discovery ST and the Philips Allegro. Both the CTI and GE products use block detector to form the cylinder of detectors. The GE Advance and Discovery ST use BGO and operate in either 2D or 3D modes by means of retractable lead septae between the rings. The CTI Reveal uses LSO and is a 3D only machine. Its count rate capability is nearly a factor of two higher than the BGO device and its coincidence window is a factor of two smaller so that random coincidences are reduced. The Philips Allegro uses GSO and therefore has similar count rate and random characteristics as the Reveal. The lower sensitivity of GSO is compensated by improved spatial resolution and by a larger axial field of view. The Allegro does not use block detectors, but has an array of photomultiplier tubes above the detectors that operate like a scintillation camera.

The performance characteristics of these scanners are shown in Table 3. The spatial resolutions are comparable as would be expected from the similarity of the crystal dimensions. The count sensitivity is best for

Table 1. Detector Properties

Property	BGO	LSO	GSO
Atomic Number	73	65	58
Density (g/cm^3)	7.1	7.4	6.7
Intrinsic Efficiency* (Section II D.2)	0.85	0.82	0.75
Coincidence Efficiency* (Section II G.1)	0.72	0.67	0.56
Energy Resolution (Section III B.)	15%	10%	8.5%
Decay Time (nsec)	300	40	60

* for 20 mm thick detector

Table 2. Whole Body PET Scanner Design Parameters

Product	Crystal Size (Number)	Axial FOV	Transverse FOV	Ring Diameter
Reveal (Accel)	6.5 × 6.5 × 25 mm (9,216)	16.2 cm	58.5 cm	83 cm
Reveal Hi-Rez	4 × 4 × 20 mm (24,336)	16.2 cm	58.5 cm	83 cm
Advance Nxi	4 × 8 × 30 mm (12,096)	15.2 cm	55 cm	93 cm
Discovery ST	6.3 × 6.3 × 30 mm (10,080)	15.7 cm	70 cm	87 cm
Gemini	4 × 6 × 20 mm (17,864)	18 cm	56 cm	90 cm

Table 3. Whole Body PET Scanner Performance Values

Product	3D Sensitivity kcps/kBq/ml	Transverse Resolution Center/10 cm*	Axial Resolution Center/10 cm*	Energy Resolution
Reveal (Accel)	57.1	6.3/7.4 mm	5.8 / 7.1 mm	25% (15%)
Reveal Hi-Rez	45	4.2/4.8 mm	4.5/5.5 mm	25% (15%)
Advance Nxi	69.7	4.8/5.4 mm	6.0 / 6.3 mm	20%
Discovery ST	78.7	6.2/6.8 mm	6.2 / 6.8 mm	17%
Allegro	44.4	4.9/5.5 mm	5.0 / 6.1 mm	16%

*Center refers to the exact center of the field of view while 10 cm refers to a point 10 cm from the center.

the BGO systems and lowest for the system with the GSO detectors.

D. HRRT (High Resolution Research Tomograph)

One other device deserves mention. The HRRT is the highest resolution human scanner in existence. The HRRT is designed for brain research and the bore diameter is only 35 cm. It has a 25-cm axial field of view and just under 60,000 2.1 × 2.1 × 7.5 mm LSO detectors in one configuration. In another design, two detector blocks are piggy-backed as shown in the picture for a total of 120,000 detectors. The front and back detectors are distinguishable by their pulse characteristics. This design allows compensation for the depth of interaction effect that is especially large because of small ring diameter. Actually, ring is not quite the right terminology because the detectors are housed in eight rectangular backs arranged as an octagon as shown in Figure 11. The spatial resolution of the HRRT is less than 3 mm, which is exceptional for a human scanner.[26, 27]

Figure 11. HRRT Brain PET System. The high-resolution research tomograph has the best spatial resolution of any human PET scanner.

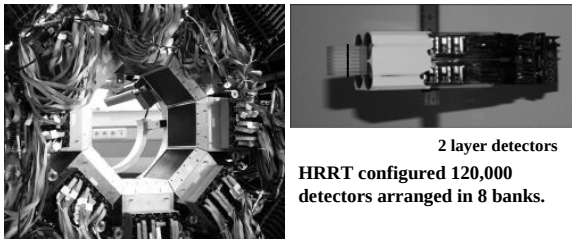

E. PET Spatial Resolution

Spatial resolution refers to the amount of blurring introduced by the imaging system. Spatial resolution is often quantified by the amount of broadening in the image of a point or line source of activity. An ideal imaging system has no blurring and produces an image of a point source as a point. A count profile taken across the point image is a delta function as shown in Figure 12. The count profile from a point image obtained on a real imaging device has a broader distribution that is referred to as the point spread function (or line spread function in the case of a line image). Spatial resolution is expressed as the width of the point of line spread function at 50% of the maximum count value. This value is called the full-width-at-half-maximum (FWHM). The FWHM values are reported in Table 3 to specify the axial and transverse spatial resolution of the PET tomographs.

Figure 12. Spatial Resolution and Full-Width-Half-Max (FWHM). Spatial resolution is quantified by the amount of blurring of an ideal point source.

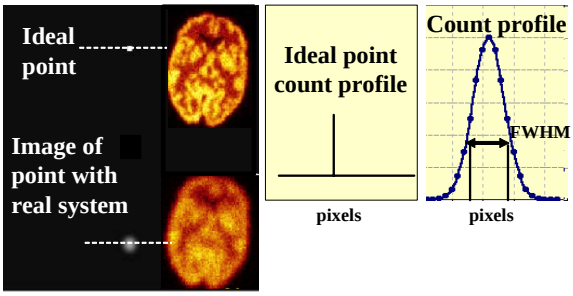

Over the past two decades, there has been enormous improvement in PET spatial resolution as shown in Figure 13. The primary factors that influence spatial resolution include the face size of the detectors, the detector thickness, the detector separation, data smoothing during or after reconstruction and the pixel size. Each of these components contributes to the overall spatial resolution of the final image. The larger FWHM components (those with the greatest blur) have the biggest influence on the total spatial resolution. Initially, the limitation was the detector size, but as detectors have become smaller the other components have had increasing importance in determining the resolution performance.[16-23]

Figure 13. PET Spatial Resolution Through the Decades. PET spatial resolution has improved over the past 3 decades with the use of improved scintillators and smaller detectors.

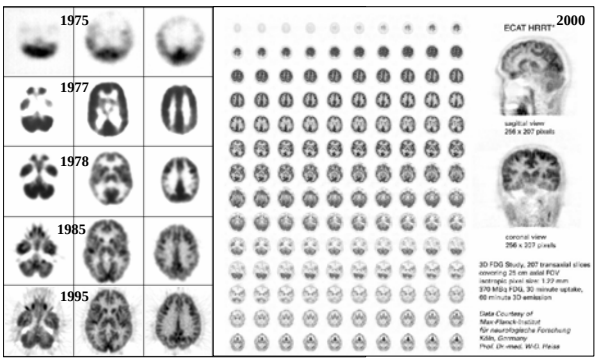

E.1 Detector Face Size

PET tomographs achieve spatial resolution through coincidence detection. Since both annihilation photons must strike the opposed coincidence detectors, the source must be located in the volume defined by the geometry of the detectors as shown in Figure 14. A point source located exactly at the midpoint of the detector pair, has the highest geometric efficiency. As the source is moved parallel to the detector plane in either direction, the geometric efficiency falls going to zero at the edge of the detector volume. Thus, the FWHM associated with the detectors is equal to the half detector face size. This of course depends on being able to identify accurately individual detector elements. Because of the uncertainty involved in selecting the correct detector with each event, the spatial resolution is approximately equal to the detector face size.

Figure 14. Detector Size & Spatial Resolution. The face size of the detector is the primary determinant of the spatial resolution.

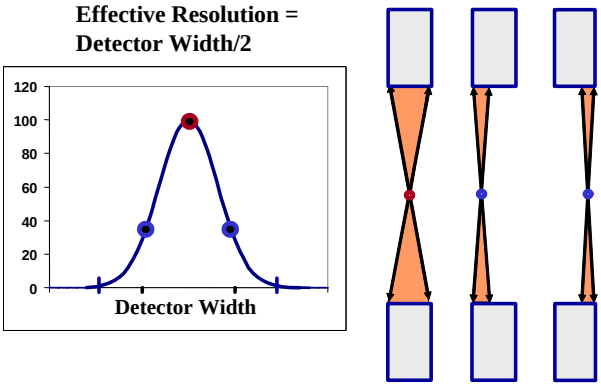

E.2 Detector Thickness

As previously discussed, high-detection efficiency is important for coincidence detection. To achieve high-count sensitivity, the detectors are typically 20–30 mm thick. When an annihilation photon strikes the detector, it can be absorbed anywhere along the detector length. Annihilation photons arriving from the center of the tomograph field of view are likely to travel along the axis of a detector and this presents no problem. However, annihilation photons coming from the edge of the field of view have trajectories that cross many detectors. Because the exact location of the interaction along the detector is not easily determined, there is a significant loss of spatial resolution. This is referred to as the depth of interaction problem and is illustrated in Figure 15.

Figure 15. Depth of Interaction & Spatial Resolution. Lack of knowledge about the interaction site in the detector causes a loss in spatial resolution.

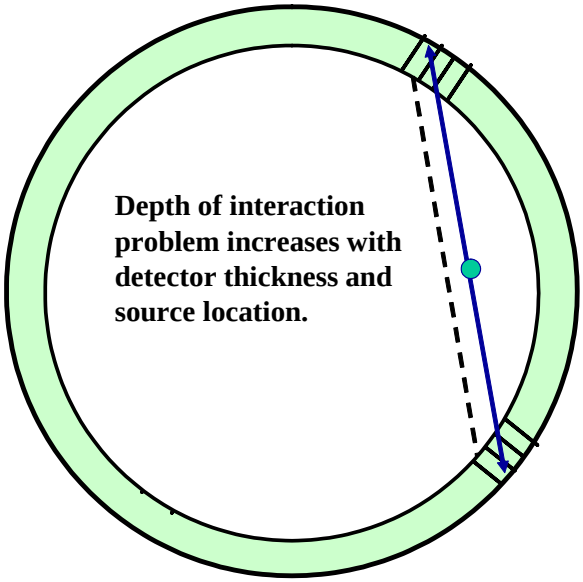

E.3 Ring Diameter

One way of reducing the loss of resolution due to this depth of interaction problem is to use thinner detectors. This is not an option with the current detectors since the detection efficiency would be seriously reduced with any reduction in thickness. Another way to reduce the depth of interaction problem is to increase the distance between the detectors, i.e., use a larger ring. There are two drawbacks associated with that approach. The geometric efficiency of the detectors decreases with the square of the

source to detector distance. Thus, a larger ring diameter results in a significant drop in count sensitivity. The other reason opposing a larger ring diameter is the loss of spatial resolution associated with the (slight) angular deviation of the annihilation photons. If the positron annihilates at rest, the angle between the two annihilation photons is exactly 180°. However, at room (and body) temperature, thermal motion adds about 0.5° (±0.25) variation in the annihilation angle. This variation produces a loss in spatial resolution that increases with the ring diameter as shown in Figure 16.

Figure 16. Non-Colinearity and Spatial Resolution. Deviations from exact 180° annihilation result in a loss spatial resolution that increases with the ring diameter.

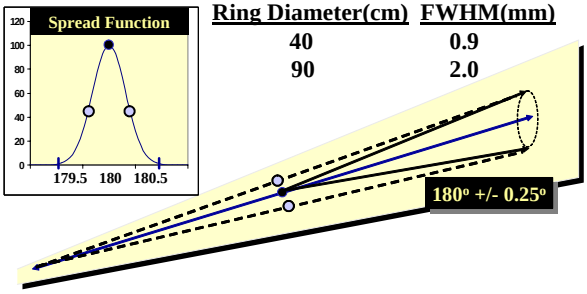

If increasing the ring diameter is not the solution for improving spatial resolution, then what is? A variety of techniques has been proposed to measure the depth that the interaction occurs. These include using layers of detectors with identifiable differences in their scintillation properties (like the HRRT in Figure 11) or by treating the surface of the crystals so that the light yield is depth dependent. So far, none of these approaches has been incorporated into commercial devices, but that can be expected in the near future.

The spatial resolution components discussed above can be described as intrinsic because they are fixed by the design configuration of the PET tomograph. The other factors that influence spatial resolution, smoothing, and pixel size vary depending on selections that the operator makes.

E.4 Data Smoothing

The PET projection information acquired during a patient study has statistical fluctuations that are part of the fundamental nature of radiation and detection. These fluctuations are amplified during the reconstruction process and as a result, mathematical operations that smooth the projections are often required. Smoothing causes blurring and must be included as a spatial resolution component. The amount of smoothing required depends on the acquired count density with low count density data needing more smoothing. Smoothing filters (kernels) are often characterized by a width that is analogous to the spatial resolution FWHM.

E.5 Pixel Size

The reconstructed images are typically presented as 128 × 128 images. In order to maintain the field of view that encompasses the patient, the pixel size is usually about 4 mm. That pixel size is associated with an 8 mm FWHM spatial resolution component and sometimes the pixel size is the primary determinant of the overall spatial resolution. Ideally, the pixel size should be selected so that it is not a significant factor. However, reducing the pixel size either requires the reduction of the field of view or a larger matrix. Using a 256 × 256 matrix would reduce the pixel size while maintaining the field of view, but would take a factor of 4 more in reconstruction time. As computer power continues to evolve with more efficient algorithms, the use of larger matrices is likely to be the preferred solution for maintaining spatial resolution and field of view. Figure 17 shows the effect on spatial resolution from the use of too large a pixel size.

Figure 17. Pixel Size and Spatial Resolution. Spatial resolution is limited by the size of the pixels used in the reconstruction.

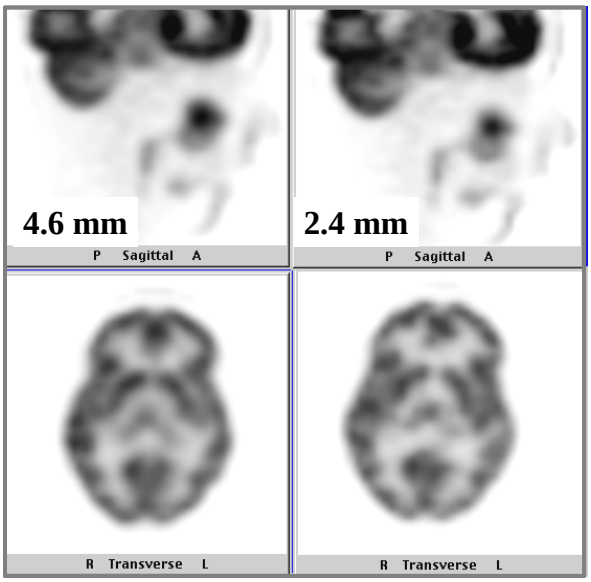

E.6 Positron Range

A final consideration with PET spatial resolution is the range of the positron in tissue before annihilation. Low energy positrons such as those emitted by F-18 do not travel far and have a negligible effect on spatial resolution. The positrons emitted by Rb-82 are very energetic and the degradation in spatial resolution is very apparent even in whole body PET scanners. The range of the positron is likely to be the limiting factor in small animal PET imaging.

F. SPECT/PET Systems

The successful application of F-18 FDG in tumor imaging prompted investigations about the potential for SPECT imaging. While SPECT imaging of positron emitters is possible, the required high energy collimation for the 511 keV annihilation photons results in poorer spatial resolution and much lower count sensitivity than SPECT imaging with conventional Tc-99m radiopharmaceuticals. Because the most common configuration for SPECT systems had two scintillation cameras that were opposed at 180 degrees, the old idea of removing the collimators and using coincidence detection was revived. The idea of adding coincidence capability to a dual detector SPECT system is attractive since the device is then able to acquire either SPECT or PET studies. PET studies are acquired like SPECT studies except that the collimators are removed and the projection views are generated from the event locations on the two detectors associated with the coincidence event. (Figure 18).[28-32]

Figure 18. Coincidence Scintillation Cameras for Pet/SEPCT. Opposed scintillation cameras can be run in a coincidence mode to provide PET on SPECT systems.

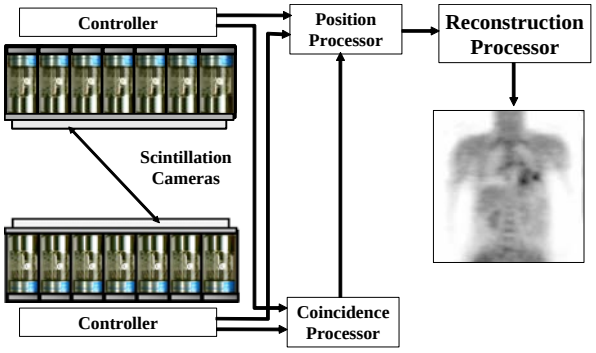

G. SPECT/PET Challenges

There are several advantages to coincidence imaging over collimated imaging of positron emitters. The intrinsic spatial resolution is much better than the SPECT spatial resolution and rivals that of dedicated PET systems. In spite of the very thin NaI(Tl) crystals used in scintillation cameras, the coincidence sensitivity also is better than that of the collimated system. There are several significant limitations, however. The coincidence efficiency for 511 keV with the thin NaI(Tl) crystals used on scintillation cameras is very low (< 10%). With the collimators removed the large area of the detector results in a very high event rate. Scintillation cameras designed for SPECT typically operate with a maximum count rate of 200–300,000 counts per second (cps). This

singles rate restricted the amount of activity that could be in the patient to several hundred micro curies and resulted in a coincidence rate of less than 1,000 cps. Because of the market opportunity represented by PET imaging, all the SPECT vendors redesigned their SPECT systems so that they would be better suited for coincidence operation. The detector thickness was increased from 9.5 mm to 13 mm and even to 25 mm in some products. In addition, the count rate capability was increased up to 2,000,000 cps. These changes resulted in systems that could image with a maximum coincidence rate in the range of 10,000 cps. In spite of these efforts, the performance of the coincidence scintillation camera systems falls well below that of the dedicated PET systems. This has been recognized by the Centers for Medicaid Services (CMS), which has restricted reimbursement for a number of PET studies to dedicated PET scanners. As a result, interest in the SPECT/PET hybrid systems has been considerably muted.

H. C-PET

One device that deserves mention here is the Philips C-PET system. This is a dedicated PET only system based on scintillation camera technology. There are six individual scintillation cameras with 25-mm thick NaI(Tl) detectors. The detectors are curved so that when they are combined they form a complete cylinder with a diameter of 90 cm and an axial length of 25 cm (Figure 19). The C-PET operates as a 3D PET system and is less expensive than the ring systems with individual detectors. It has spatial resolution that is comparable to the ring detector systems and much better energy resolution. However, its count sensitivity is about half that of the ring systems. It is considered by CMS as an instrument that is reimbursable for all the approved PET studies.[33]

Figure 19. C-PET System. This is a dedicated PET system that uses NaI(Tl) scintillation cameras as the detectors.

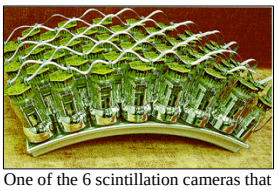

One of the 6 scintillation cameras that make up the C-PET system. Sensitivity and count rate capability are limitations associated with this device

IV. PET CORRECTIONS

There are a number of corrections that have to be made to the acquired PET data before it can be reconstructed. These include corrections for sensitivity variations, random coincidences, scatter, and attenuation.

A. Sensitivity

The reconstruction algorithm requires a set of measurements that provides projections of the radionuclide distribution from a large number of angles. Changes in the measured count rate should only depend on the in vivo radioactivity distribution and not on variations in the detectors. It is not possible to have all 10,000+ detectors with uniform sensitivity, so there is some variation from detector to detector. However, even if the detector response was 100% uniform, there would still be a need to do a sensitivity correction. This is because both the geometric and intrinsic efficiency vary with the angle of the line of response. A coincidence event that occurs across a ring diameter has a significantly higher chance of being recorded than one that takes place between detectors that are closer together. This is illustrated in the Figure 20. To compensate for both this angular dependence and for other variations in the detectors, sensitivity scans are acquired as part of the daily quality control. These scans are acquired either

using a transmission source or with a uniform cylinder of radioactivity.

Figure 20. Sensitivity Variations. The sensitivity of the coincidence lines of response depends on the location of the detectors within the ring.

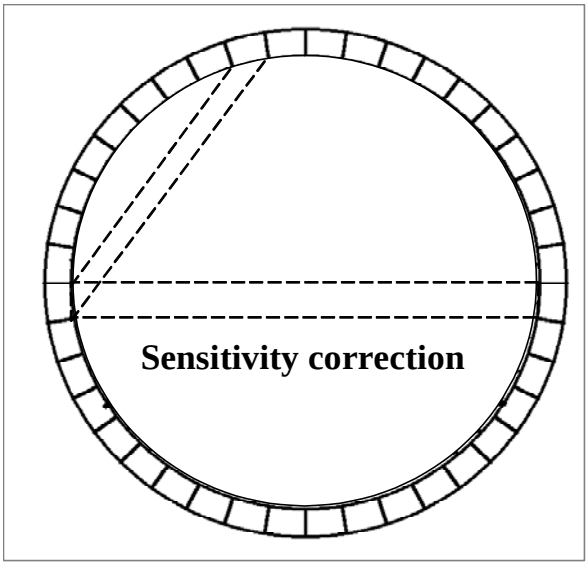

B. Random Coincidences

The random coincidence rate increases with the square of the singles count rate so it can be a substantial fraction of the acquired counts especially in 3D PET. Unlike scatter, the distribution of random coincidences is not strongly source dependent and they tend to be dispersed over the entire imaging field. Random coincidences can be estimated from the singles rate or measured by introducing a time delay into the coincidence circuit. A time window set on this delayed signal will only sample the random coincidences (Figure 21). The estimated random events are usually subtracted from each line of response prior to reconstruction, although some iterative algorithms include this step as part of the reconstruction process.[16-19,22]

Figure 21. Random Coincidence Estimation from Time Spectrum. True coincidence events occur over a limited time interval while randoms are uniformly distributed.

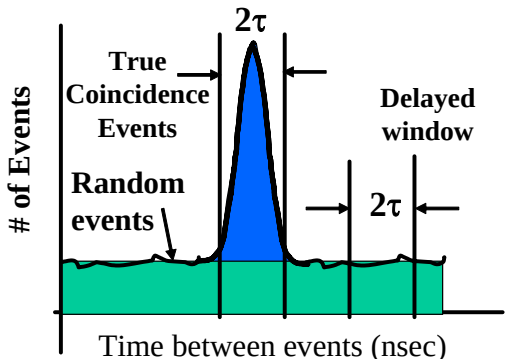

C. Scattered Radiation

The annihilation photons traveling through the patient are attenuated largely through Compton scatter interactions. With Compton scatter, the primary photon suffers a billiard ball like collision with a loosely bound electron. The scattered photon resulting from this interaction loses energy and changes its direction. The energy of the scattered photon depends on the angle of the scattered photon relative to the primary photon. Detection of the scattered photon causes a loss of spatial resolution and image contrast because the location of the event is not correctly registered as shown in Figure 8. If the energy resolution of the detectors is good, a portion of the scattered events can be eliminated by setting a tight energy window.

Scattered radiation is easily handled in 2D PET studies because the scatter contribution is about 10–15% of the acquired events. The scatter component is estimated by fitting the recorded counts that extend beyond the patient boundary to a parabolic or Gaussian function in each projection (Figure 22). The fitted function is subtracted from the projection. While this is approach is not rigorous, it is sufficiently accurate in the 2D mode.

Figure 22. 2D Scatter Correction Methods. The obvious scatter events beyond the edge of the projections are used to fit an estimated scatter function.

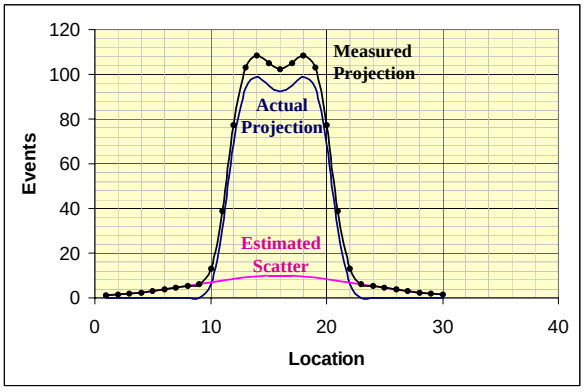

Scatter correction in 3D PET is complex. Scatter is estimated from an algorithm that models the transport of photons through the patient. The amount of scatter contaminating any given line of response depends on the activity distribution and the attenuation map of the patient. Therefore, in order to compute the scatter using this method, both the transmission data and the scatter-contaminated PET data have to be reconstructed. The resultant images are used to estimate the amount of scatter that is contributed to each line of response. The scatter component is subtracted and the corrected data is then presented to the reconstruction algorithm. Even though this approach appears to work well enough, although it has been adapted on the commercial PET systems, there is still room for improvement. This approach only corrects for activity in the FOV. In many cases, there is significant scatter that originates outside the field of view. In addition, the current approach assumes that the annihilation radiation has only one scatter interaction. More sophisticated algorithms are being explored that will expand the range of the correction to include the aforementioned cases. However, the ideal solution is to have better energy resolution so that scatter can be eliminated during the acquisition.[24, 34-38]

C. Attenuation Correction

Annihilation radiation like x-rays and gamma rays become less intense as they travel through material objects. The loss of photons from the beam is referred to as attenuation. For annihilation radiation, attenuation in the body is primarily due to Compton scatter interactions. Attenuation is exponential and as a result, we can define a quantity called a half value layer (HVL). The HVL is the thickness of material that reduces the intensity of the radiation by ½. For soft tissue (water), the HVL for annihilation radiation is 7.2 cm. In order for a coincidence event to be recorded, the two annihilation photons have to hit opposing detectors. The amount of attenuation along any line of response therefore depends on the total path length through the patient irrespective of where the source is located. For the line of response shown in Figure 23, the coincidence attenuation reduction is the same for all three sources.[18, 24, 39]

Figure 23. Path Dependence of Attenuation. Since both annihilation photons must be detected for a coincidence event, the attenuation path is the total distance between the two detectors.

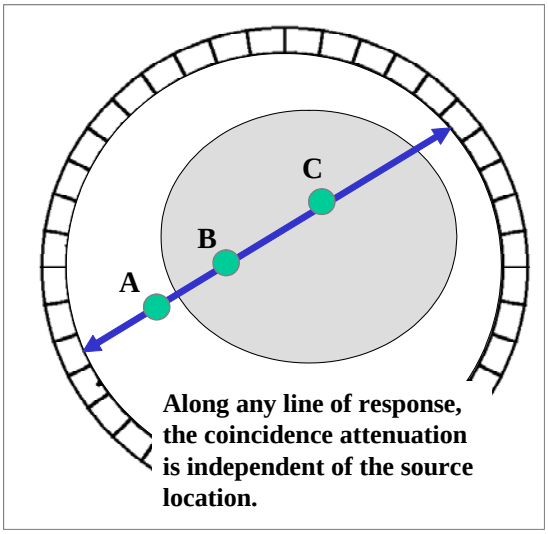

C.1 Attenuation Artifacts

Trajectories that just graze the edge of the patient have essentially no attenuation. Trajectories that traverse the thickest portion of the patient can have path lengths of greater than 50 cm in large patients leading to reductions in the coincidence detection rate of more than a factor of 100. The information acquired by the PET tomograph represents the number of detected annihilation photons emitted from the patient. This number depends on the activity of the positron emitting radionuclide distributed in the patient and the patient attenuation. The reconstruction algorithm used to produce the PET images is based on the tacit assumption that the detected events depend only on the amount of activity. Reconstruction of the acquired data without attenuation correction leads to the characteristic artifacts as shown in Figure 24 including intense activity at the skin, increased activity in the lung fields and decreased activity in the central portions of the patient.

Figure 24. PET Attenuation Artifacts. Reconstructed PET studies that have not been corrected for attenuation have profound artifacts. High-count density in the lungs and at the skin boundaries are common manifestations.

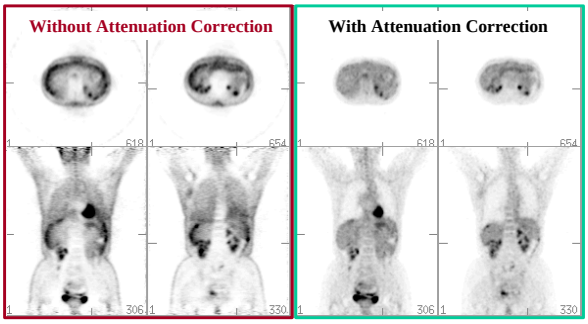

C.2 Transmission Scans

The amount of attenuation depends only on the trajectory of the annihilation photons through the patient, not on the actual location of the source. This is true even if the source is outside of the patient and this allows the measurement of the correction factors with transmission scans. As shown in Figure 25, a radionuclide source revolves about the patient to collect the transmission data. The radionuclide source is either germanium-68 (Ge-68), a source of annihilation photons, or cesium-137 (Cs-137) which emits a single 662 keV gamma ray per decay. The Ge-68 transmission measurement uses coincidence detection, which provides good localization, but is limited by the coincidence efficiency and count rate capability of the detectors. Transmission scans with Cs-137 use conventional detection (i.e. non-coincidence) and have fewer problem with count rate. Another advantage of Cs-137 is its 30-year half-life. Ge-68 sources have a 288-day half-life and need to be replaced on an annual basis. Typically, the duration of a transmission study is about 1–3 minutes per bed position.

Figure 25. Radionuclide Transmission Measurements. The PET scanner is used as a crude CT scanner to collect transmission data used for attenuation correction.

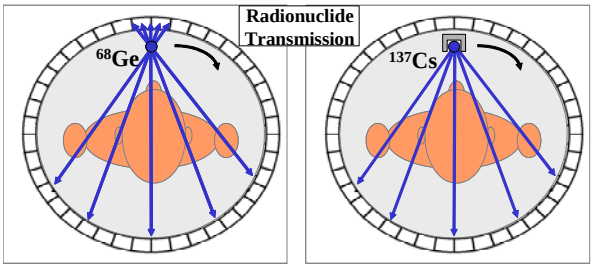

It would be most convenient to acquire the transmission measurements while the PET emission study is being acquired to reduce the study time and potential problems with misregistration between the transmission and emission scans. That is not practical with the Ge-68 source. Because of the cross talk with the administered activity, the transmission data would contaminate the emission data. The transmission measurement is performed as an additional study for

each bed position after the emission data is collected. Since the transmission scan contains both emission and transmission events, the emission data has to be subtracted from the transmission data. This correction increases the statistical uncertainty associated with the transmission values. Transmission measurements with Cs-137 are also performed separately from the emission scans but have several advantages. On systems with good energy resolution, the cross talk between the 511 keV annihilation radiation and the 662 keV gamma ray associated with Cs-137 can be eliminated with the appropriate energy window. Because the Cs-137 transmission is acquired conventionally, more activity can be used and a useful transmission study can be acquired in less than 1 minute per bed position.

C.3 Transmission Noise

The transmission factors for each line of response are determined from the ratio of the source counts without and with the patient in place. The corresponding emission data is multiplied by the correction factors to compensate for the effects of attenuation. The statistical uncertainty of the transmission factors is often significant and degrades the quality of the corrected emission data. One approach to minimizing this effect has been segmented attenuation correction. The transmission data can be reconstructed as a CT study to yield an estimate of local attenuation values in the patient. The noise associated with the attenuation values is reduced by averaging over portions of the scan where the attenuation is uniform. These uniform attenuation areas are determined by a segmentation algorithm as shown in Figure 26. After the segmented areas have the measured attenuation coefficients replaced by the mean value, the transmission factors are recalculated with significantly less noise.[40]

Figure 26. Segmented Attenuation Correction. Noise in the transmission scans can be significantly reduced by replacing measured attenuation values with mean attenuation values.

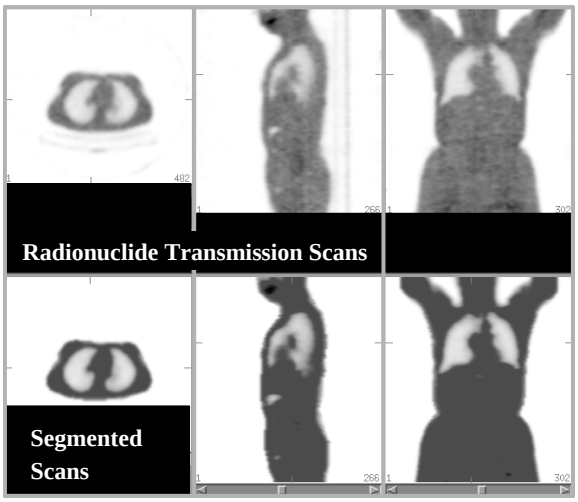

The latest improvement to attenuation correction is the combined PET/CT system where a high quality CT study provides whole body transmission data in less than 1 minute. In addition to the reduction in transmission time, the level of noise in the CT images is much less than that of the radionuclide transmission data. This is illustrated in Figure 27. However, there are several potential problems with using this data for attenuation correction. Those issues will be discussed in the PET/CT section.

Figure 27. Radionuclide and CT Transmission Image Comparison. X-ray transmission studies acquired on a CT scanner provide superior attenuation correction.

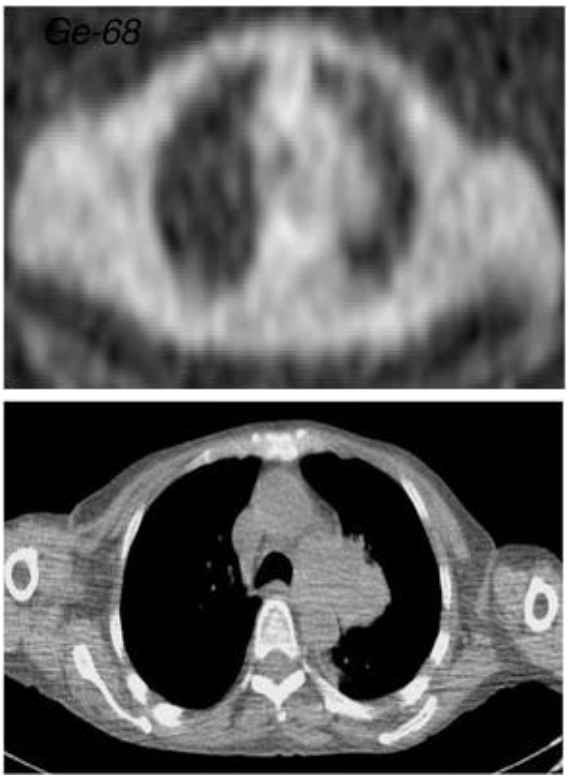

V. PET RECONSTRUCTION ALGORITHMS

For all nuclear medicine based tomographic imaging systems, the goal is to accurately reconstruct the internal distribution of tissue radioactivity concentrations from external measurements. That can be done exactly if the acquired measurements represent a complete set of line integrals through the desired planes. Put more simply (and specifically for PET), the acquired measurements should yield the sum of all the activity along each line of response. The ring design of dedicated PET scanners insures that there are enough lines of response to sample the volume to satisfy the complete set requirement. However, the detected events for the line of response do not represent the line integrals (radioactivity sums) through the planes. The main problem is tissue attenuation, which can be compensated for if the tissue attenuation map is known. Other problems include random coincidences, scattered radiation, spatial resolution, and noise. Each of these components was discussed in the preceding sections. In the following section, the reconstruction process will be discussed with the assumption that all the corrections can be accurately effected.

A. Sinograms

We will first consider the data sets obtained from 2D PET acquisition. In 2D PET, the lines of response are constrained to transaxial planes. These lines of response are usually re-organized (re-binned) into multiple sets of parallel rays to form projections that span the range from 0 to 180 degrees. When those projections are ordered by angle, they are referred to as sinograms (Figure 28). Sinograms are generated for each transaxial plane in the PET system field of view. Once they are corrected for attenuation, random coincidences, and scatter, these projections are presented to a reconstruction algorithm. The analytic approach to reconstruction is filtered backprojection while the non-analytic approach uses an iterative algorithm. Both of these rely on a mathematical operation called backprojection.[18, 24, 41]

Figure 28. Projection Data Required for Reconstruction. All reconstruction algorithms require a complete set of projections.

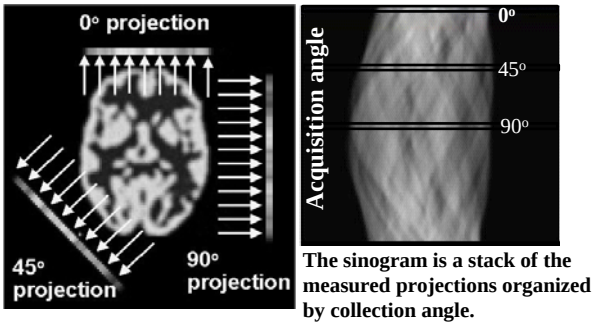

The sinogram is a stack of the measured projections organized by collection angle.

B. Backprojection

Backprojection is a conceptually simple idea. Acquired (and corrected) projection data are added to an image matrix along the angle that they were collected. This is illustrated graphically in Figure 29.

Figure 29. Backprojection. Backprojection is a mathematical operation used in all reconstruction algorithms.

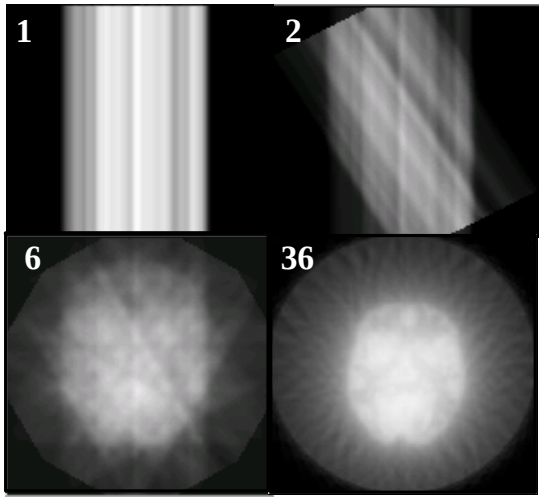

Numbers indicate the number of projections backprojected.

C. Filtered Backprojection

Backprojection yields a low contrast, blurred distortion of the tomographic image. In 1917, the mathematician Radon discovered that this distortion could be eliminated if the projection data were modified prior to reconstruction by a specific filter often called the ramp reconstruction filter. Because this process involves the ramp filtering of the projections followed by backprojection it is referred to as filtered backprojection (Figure 30). Filtered backprojection was widely used in PET over the past decade because it produces high-resolution images and it is very fast. However, it does have several disadvantages. Corrections for attenuation, scatter, and randoms must be done before reconstruction. It is also susceptible to noise and frequently will have prominent streak artifacts when there are high activity concentrations in the image. Over the last 5 years, iterative algorithms have supplanted filtered backprojection.

Figure 30. Filtered Backprojection. If the projections are modified with a ramp filter prior to backprojection, true tomographic images will be obtained if the projections are accurate and complete.

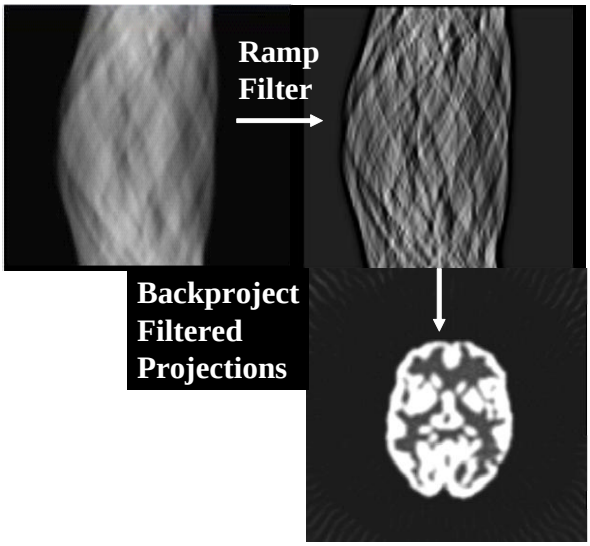

D. Iterative Algortithms

With iterative algorithms, the tomographic images are reconstructed by successive approximations as shown in Figure 31. Initially, it is assumed that the tomographic image has a uniform radioactivity concentration. From this starting point, the algorithm calculates the sinogram that the imaging system would have measured on the assumed starting image. This step is called forward projection and one can incorporate all the physics of the imaging process into it such as attenuation and scatter. The result of the forward projection is compared to the measured sinogram. For the class of iterative algorithms most often used in PET, this comparison is simply the ratio of the measured and calculated sinograms. Other iterative algorithms such as those used in the initial CT scanners use the difference between the two sinograms. The result of the comparison is backprojected to yield a correction update. The update is multiplied into the

tomographic image to complete the iteration. This process continues until some stopping criteria are met. The algorithm described is called the expectation maximization maximum likelihood algorithm (EM-ML).

Figure 31. Iterative Reconstruction Algorithms. Reconstruction is obtained through a set of successive approximations governed by the comparison between the measured projections and the projections calculated from the current estimate.

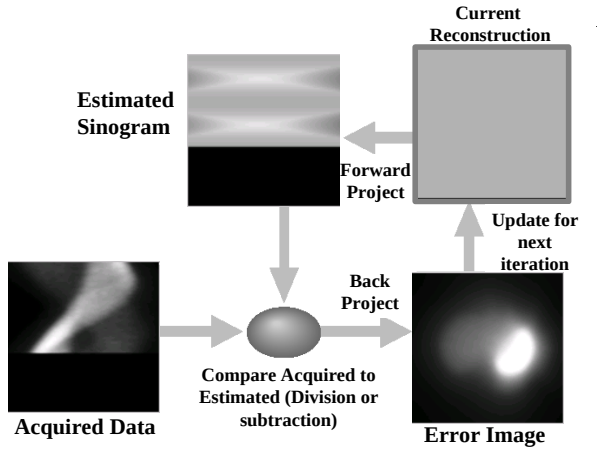

E. Ordered Subsets

The EM-ML algorithm has many nice properties, but it is very slow to converge and often requires more than 20 iterations. In 1995, Hudson and Larkin developed ordered subsets expectation maximization (OS-EM), an iterative technique based on the EM-ML algorithm that split the sinogram into subsets (Figure 32). The EM-ML algorithm is applied to each subset and one iteration is completed when all the subsets have been operated on. To go through all of the subsets takes about the same processing time as an iteration of the EM-ML algorithm, but because the reconstructed image has been updated for each subset, convergence is much faster. For most PET studies, 2–3 iterations of the OS-EM algorithm are sufficient.

Figure 32. Projections Reorganized as Ordered Subsets. The iterative algorithm operates on a portion (subset) of the data resulting in faster convergence.

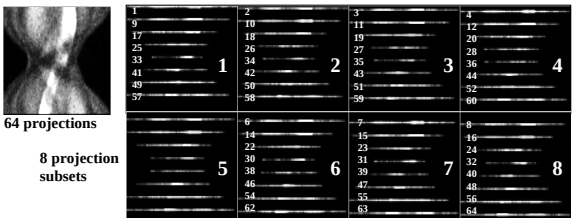

F. 3D PET Reconstruction

As noted above, the direct plane information obtained from 2D PET direct planes is sufficient to reconstruct accurately the information in the PET tomograph field of view. 3D PET removes the between plane restrictions and allows coincidence detection between rings as well as the direct planes thereby increasing the sensitivity by a factor of four or larger. Incorporating this extra information into the reconstruction algorithm presents a challenge even if one ignores the problem of scatter and randoms. Colsher proposed the first successful solution to the 3D PET reconstruction problem in 1980. He developed a 3D filtered backprojection algorithm that is analogous to the 2D version and defined the appropriate reconstruction filter. This filter, commonly referred to as the Colsher filter is two-dimensional and it is applied to the PET data organized as projection views. The projection view is a stack of the projection for each axial plane for a given angle very much like the projection view acquired from a SPECT camera. However, in order for the 3D filtered backprojection to work, every point in the object volume must be uniformly sampled. This does not occur for large objects because of the limited axial field of view of the scanner. A solution was found for this problem, but it is computationally expensive. The object is first reconstructed only using direct planes. The missing planes can then be calculated and added

to the data set making it suitable for the 3D filtered backprojection algorithm. This approach is called PROMIS (PROject MISsing data). Initially this approach was too time consuming to be clinically practical and other approaches were investigated. The method that all current vendors support uses Fourier rebinning.[24, 41]

F.1 Fourier Rebinning

3D PET records data from between distant detector rings as well as from the direct planes. As illustrated in Figure 33, the data from non-adjacent rings cross many direct planes. If there were a way to accurately and efficiently add the contribution of this data to the direct planes, the reconstruction problem would be reduced to a 2D filtered backprojection or OS-EM. Fourier rebinning accomplishes that with sufficient accuracy for current PET imaging. Examples of 3D studies reconstructed using Fourier rebinning on 3D PET are compared with 2D PET studies acquired on the same patient in Figure 34.[24, 41-44]

Figure 33. 3D Fourier Rebinning for Reconstruction. Information from the oblique sinograms is added accurately to the direct plane sinograms so that conventional reconstruction algorithms can be used.

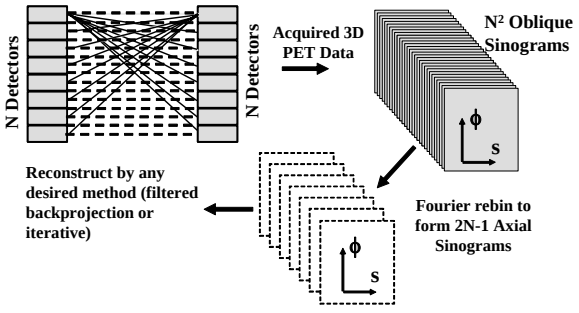

Figure 34. 3D Fourier Rebinning for Reconstruction. These images compare 3D PET using Fourier rebinning with 2D PET on the same patient.

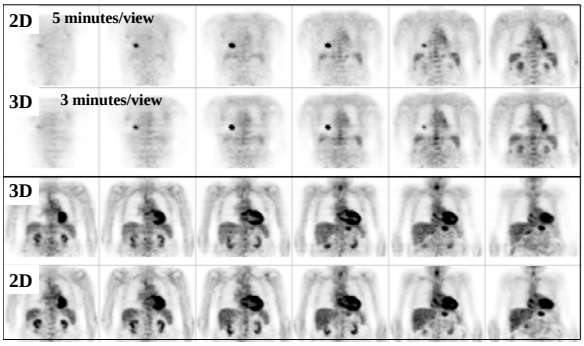

F.2 RAMLA

Although Fourier rebinning works very well for brain imaging and adequately for whole body imaging, better reconstruction algorithms are under constant investigation. Most of the effort is devoted to three-dimensional iterative algorithms. Currently, Philips offers a 3D iterative approach referred to as a row action maximum likelihood algorithm with the acronym RAMLA. RAMLA is an accelerated maximum likelihood algorithm similar to OS-EM but it has an additional parameter that controls the convergence. The RAMLA algorithm used by the Philips device has an additional feature where it models the data as volumetric "blobs" instead of voxels. The size and shape of the blobs are controlled by parameters that can be adapted to the quality of the data. This approach has been shown to produce superior reconstructions when compared with conventional voxel data representation. The images produced by 3D RAMLA reconstruction are superior to those resulting from Fourier rebinning, however, the reconstruction time is significantly longer. Examples of images from the two systems are shown in Figure 35.[24]

Figure 35. Fourier Rebinning Compared With 3D Iterative (RAMLA)

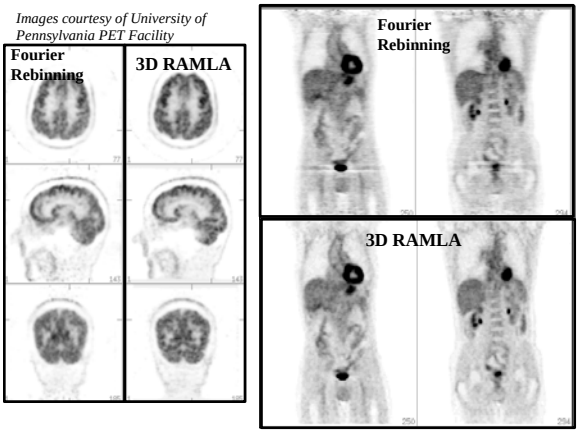

F.3 MAP Routines

Iterative algorithms can incorporate information about spatial resolution and scatter to improve reconstruction, but is there more that can be added? The answer is yes. It is possible to include additional information into the algorithm that will yield a better result. One class of iterative algorithms that accomplishes this is the maximum a posteriori (MAP) routines. Constraints can be added into MAP algorithms if they satisfy certain mathematical requirements know as Gibbs priors. As a result, smoothing constraints and even anatomical information from co-registered CT of MRI studies can be incorporated into the algorithm to improve image quality. This is an area of active research and although no commercial algorithms exist for human studies, it is likely that they will be available in the near future for the small animal PET systems.[45-48]

VI. 2D vs. 3D PET

Commercial PET systems were originally designed as 2D only systems. These systems did not have the electronic capability to handle the high event rates associated with 3D PET imaging and they did not have the practical means to reconstruct 3D data or correct for scatter. As these capabilities became available in the last decade, whole body PET systems went from being 2D only, to combined 2D and 3D devices to finally 3D only. Currently, only the GE products have the capability of performing 2D PET.

A. 2D PET Design

2D PET systems have lead septae between the rings to restrict the lines of response. This allows coincidence events to be collected within a ring (direct plane) and coincidence events between adjacent rings (cross planes) (Figure 36). Because of the shallow angle that is associated with the cross plane events, these are treated as if they came from a direct plane mid-way between the two planes. As a result, the conventional filtered backprojection algorithm can be used to quickly reconstruct 2D PET data.

Figure 36. 2D PET Sampling. 2D PET systems acquire coincidence lines of response within the plane of a ring (direct planes) or between adjacent rings (cross planes).

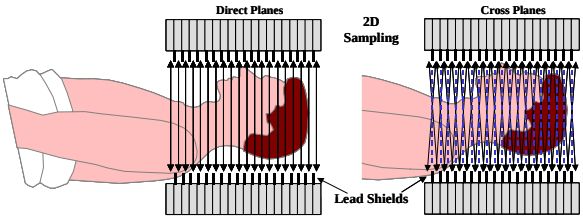

In addition to restricting the lines of response, the shields have several beneficial aspects. Because the overall event rates (both singles and coincidence) are reduced, the electronics can be simplified. The reduction in the singles count rate automatically means that the random coincidence rate is less and count rate losses due to dead time are less of a concern. Scattered radiation is also reduced in the 2D mode with the scatter fraction being about 15% of the true coincidence data. As a result, corrections for scatter do not need to be extremely accu-

rate and approximate routines that are fast can be used. 3D scatter correction is very complex and is the most challenging part of the corrections. Imaging in the 2D mode places the highest premium on intrinsic efficiency since the effects of scatter and count rate are reduced by the shields and BGO is clearly the preferred detector material.

B. 3D PET Design

3D PET offers the advantage of much higher count rate when the lead shields are removed and coincidences are allowed between all the rings (Figure 37). The higher count rate allows higher patient throughput and potentially lower radiation dose to the patients. However, there are also many challenges associated with the increased event rate that occurs when the shields are removed. Both the random coincidence and scatter events increase dramatically. The scatter fraction approaches 50% of the true coincidence rate with a similar ratio for the randoms. In addition, count rate losses resulting from detector dead time also become a concern. While BGO is the clear choice for 2D PET, its poor energy resolution and large dead time make it less attractive in 3D. LSO and GSO on the other hand make up for their diminished intrinsic efficiency with improved energy resolution and higher count rate capabilities.[16,17,22,41]

Figure 37. 3D PET Sampling. With 3D PET, coincidence lines of response can be between any of the rings.

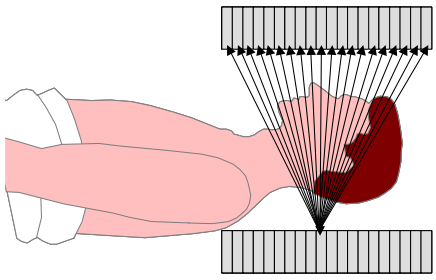

B.1 3D Sensitivity

Although the overall sensitivity increases in 3D PET, there is a position dependence that is not an issue in 2D PET. A source located in the in the center of the cylinder interacts with all the rings as shown in Figure 38. As the source moves toward either end, the number of rings decreases along with the sensitivity. The sensitivity profile in 3D has a triangular shape. To compensate for this characteristic, there is a 30–50% overlap of the bed translation during whole body scans.

Figure 38. 3D PET Sensitivity Profile. Because of the coincidence geometry, the sensitivity is maximized for central sources and decreases linearly as the sources move away from the center.

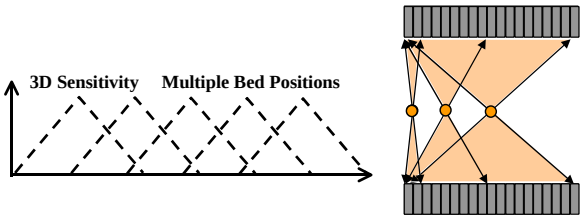

Comparisons of 2D and 3D PET modes cannot be made solely based on the measured count rates. As discussed above, the increase in count rate in 3D is accompanied by increases in the magnitude of corrections for both randoms and scatter. To illustrate meaningful comparisons, the concept of the noise equivalent count rate is used.

B.2 Noise Equivalent Count Rate

The emission and detection of annihilation photons are governed by Poisson statistics. This means that the statistical precision of the projections depends on the number of detected events. The precision is proportional to the square root of the number of events. If 100 events are detected, the precision is 10% and the precision is 3.2% for 1000 events. Increasing the number of detected events is the prime motivation for 3D

PET. As has been discussed, not all the events that are acquired on a PET system are useful. Random coincidences and scatter degrade image quality and should be eliminated. Removal of these events increases the statistical fluctuations in the projections. The noise equivalent count rate (NEC or sometimes NECR) is a way of comparing the actual gain associated with an increased of sensitivity that also requires increased corrections. The NEC can be expressed in terms of the true coincidence count rate (the good data, usually represented by T) and the scatter count rate (S) and the random coincidence rate (R):

$$NEC = T^2/(T+S+R)$$

For 2D PET, the scatter fraction is about 10% of the acquired events and a typical random coincidence rate is 25% of the acquired events. In 3D PET, both the scatter fraction and the random coincidence rate are close to 50% of the true coincidence rate. Therefore, even though the observed rate goes up by more than a factor of six in going from 2D to 3D PET, the improvement in NEC is between three and 4 (Figure 39). The NEC is also useful in comparing the performance of the different 3D PET systems.[18, 19, 23]

Figure 39. NEC Comparison of 2D and 3D PET. (Shaded area is clinical activity range).

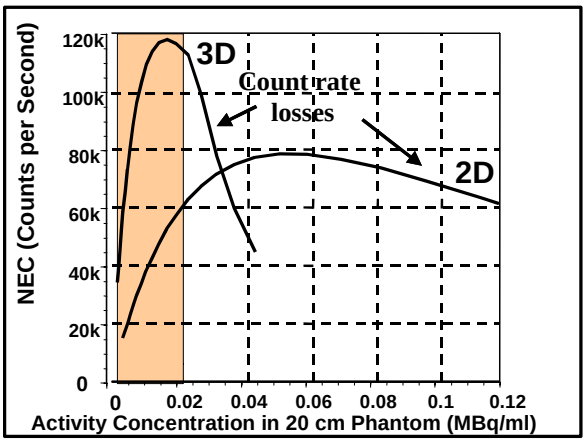

VII. PET/CT

The combined PET/CT systems were developed at the University of Pittsburgh by Townsend et al. and were initially introduced as commercial devices by CTI in collaboration with Siemens. The other two major diagnostic equipment manufacturers, General Electric (GE) and Philips quickly followed with their own devices. In each case the vendor has combined a high quality dedicated whole body PET scanner with a high quality CT scanner (Figure 40). Even though there are essentially only three vendors, the mix of models that have been released is a little confusing. Table 4 below summarizes what currently is available.

Figure 40. Commercial PET/CT Scanners.

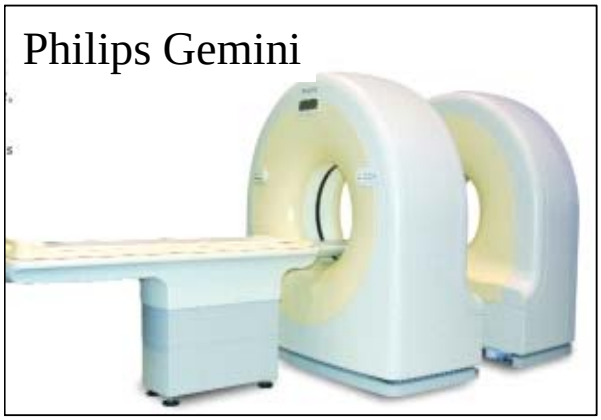

In all 3 designs, the CT scanner is at the front and the PET scanner at the rear.

Table 4. Commercial PET/CT Systems

Manufacturer	Product	CT	PET
CPS (CTI & Siemens)	Biograph Reveal RT	Somaton Emotion 2, 6 slice	Reveal Hi-Rez
		Somaton Sensation 16 slice	Reveal RT ECAT Accel
General Electric	Discovery LS	Lightspeed 4, 8, 16 slice	Advance Nxi
	Discovery ST	Lightspeed 4, 8, 16 slice	Discovery ST
Phillips	Gemini	MX8000 2, 16 slice	Allegro

In case it is not clear, the Reveal RT and the Biograph are the same instrument; CTI and Siemens have given them different marketing names. These devices were originally released with the Emotion CT. GE released the Discovery LS with the 4- and 8-slice Lightspeed CT. This prompted CPS (the collaborative union of CTI and Siemens) to release their system with the 16-slice Somaton Sensation. Predictably, GE and Phillips have also provided 16-slice capability. The Gemini system has the distinguishing feature that

it can physically separate the CT and PET portions of the system as can be seen in Figure 40.[49-54]

A. PET Systems

Tables 2 and 3 in the PET Design section summarize the PET systems that are provided for the different PET/CT systems. Several interesting trends are apparent. Both GE and CPS have opted to go for higher throughput with the loss of some spatial resolution. The Reveal/Accel and the Discovery ST use detectors with larger face size than their previous models. The Discovery ST also has reduced the thickness of the lead septae to improve the count sensitivity in the 2D mode. Examination of the whole body images does not show any appreciable difference from these changes. This result is consistent with the relatively coarse pixels that are used in whole body imaging and the available count density, both of which limit the achievable spatial resolution.

B. Combined PET and CT Systems

Currently, the combined PET/CT systems are the hottest items on the market. There are several compelling reasons for this. The quality of the PET images is significantly improved by the CT transmission correction. The CT transmission study is much faster than the radionuclide transmission so that studies are completed in about half the time of the PET only systems. This shortened scan time not only provides for higher patient throughput, it decreases the artifacts associated with patient motion. It is worth noting that multi-slice CT systems are actually required for the transmission studies, since conventional CT scanners have tube loading restrictions that limit the length of the body that can be scanned. Single slice and even dual slice CT scanners may require time for the x-ray tube to cool before a whole body transmission scan can be completed.[55-59]

C. Co-registration

The other obvious advantage to PET/CT systems is the availability of accurately co-registered images (Figure 41). All the vendors have convenient viewing software that allows the simultaneous review of the PET, CT, and fused co-registered image sets. The viewing physician can localize an area of concern on any one of the displays and immediately see the corresponding location on the other views. Several groups have shown that information displayed in this manner provides gains in sensitivity, specificity, and confidence of interpretation especially for the less than experienced reader. Although co-registration of PET and CT is possible with data sets acquired on different systems, the practical implementation is often difficult. Problems include different body orientations (e.g., arms up on one scan, arms down on another), breath hold conditions, and access to both data sets. [60-62]

Figure 41. Examples of Co-registered Image Sets from PET/CT Systems.

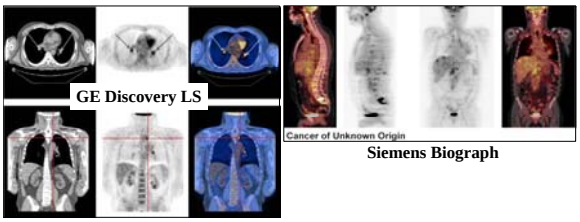

Siemens Biograph

D. PET/CT Disadavantages

There are disadvantages that have to be considered. The cost of a PET/CT system is at least 50% higher than a PET only system. A much larger room is required so that the patient can be fully translated through both devices. The radiation dose to the patient from the CT acquisition is about 1300 mrem compared to 75 mrem for a radionuclide transmission study. In addition, additional technologist training is required for operating the CT scanner. Other issues related to technologist training and health care personnel include the use of contrast. Intravenous

contrast studies have not been widely used on PET/CT at this time. This affects the diagnostic information available from the CT study. As more experienced is gained in the use of PET/CT this is likely to change.

E. PET/CT Artifacts

This section on PET/CT closes with a discussion of some of the artifacts, with which users should become familiar. Most of these concern problems associated with the CT transmission correction. As a result, many users are routinely viewing the PET studies that have not been corrected for attenuation to help alert them to these problems.

E.1 CT Field of View Truncation

The useful field of view for CT scanners is limited to 50 cm. Most patients can be accommodated easily into this field size if the arms are positioned above the head. Unfortunately, the relatively long PET portion of the study makes this difficult for some patients. For large patients who cannot tolerate an arms-up position, the arms have to be positioned on top of the thorax, since they will go outside of the CT field of view if positioned at the sides. When substantial portions of the body are out of the field of view, artifacts occur like those shown in Figure 42.[53]

Figure 42. Artifact from CT Field of View Truncation.

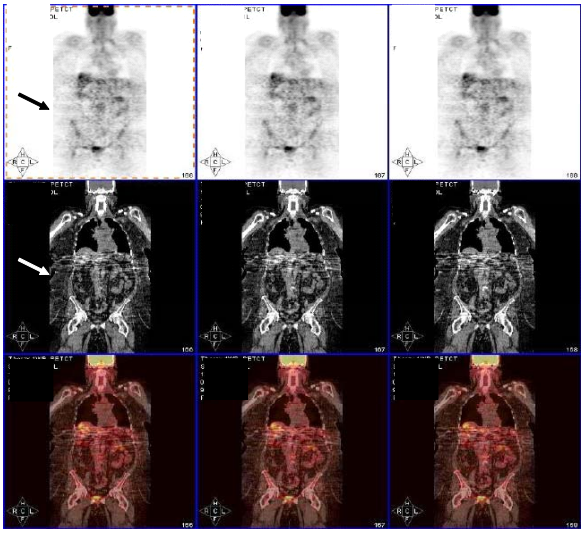

E.2 Breathing Artifacts

The PET portion of the study is acquired over several minutes for each bed position with the patient breathing normally. The CT is acquired as a spiral scan and requires the patient to hold their breath. In CT clinics, the patients are often told to take a deep breath and hold it. Because of the large capacity of the lungs, this approach destroys the registration of entire thorax and creates severe artifacts. Ideally, the patient should take a shallow breath that approximates the lung volume under normal breathing. This requires patient cooperation and not all are capable of providing it. Breathing during the spiral CT scan creates artifacts in both the CT and the attenuation corrected PET studies as shown in Figure 43.[53, 63, 64]

Figure 43. Breathing Artifact. The separated or mushroom liver is a common artifact that occurs if the patient is breathing during the CT transmission study.

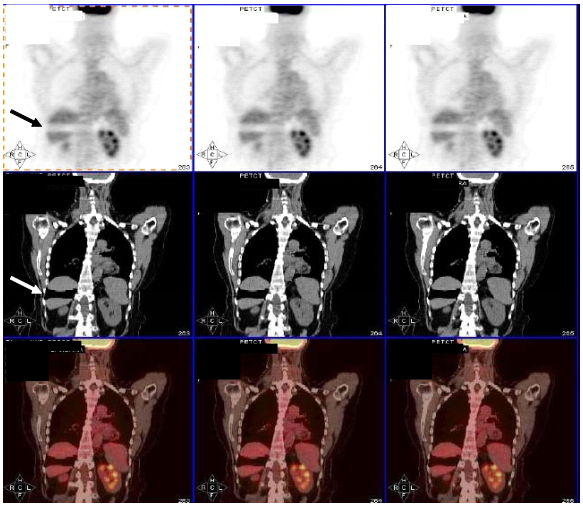

E.3 Contrast Artifacts

Although the x-ray energies are nearly an order of magnitude less than the PET annihilation radiation, it is possible to map the CT attenuation coefficients to PET attenuation values in a more or less direct manner. While a discontinuity occurs for bone, this is well compensated by the mapping algorithm. Oral or IV contrast with iodine or barium is not adequately accounted for in that simple mapping. This will cause artifacts unless it is compensated for properly. These artifacts do not appear to be much of a problem with diluted oral contrast.[24, 53]

E.4 Metal Artifacts

Metal causes rather severe artifacts on CT images and therefore artifacts on PET studies (Figure 44). The problem is widespread particularly in the mouth since so many people have dental fillings. Another area of concern is artificial joint replacements. A potential solution to this problem is the use of more sophisticated CT reconstruction algorithms that reduce or eliminate metal artifacts. However, these are not widely available on the commercial CT units used in PET/CT. As a result, many clinics are routinely reconstructing and viewing uncorrected (i.e., no attenuation correction) as well as corrected studies to overcome the problems associated with metal artifacts.[24, 53]

Figure 44. Metal Artifact from Gold Crown. The reconstructed study without attenuation correction can be used to identify metal artifacts.

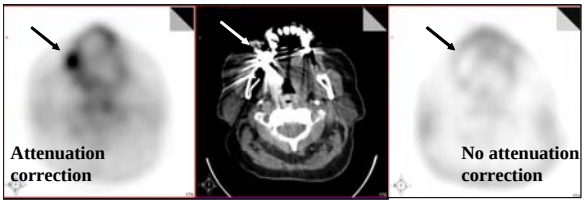

VIII. SMALL ANIMAL PET SYSTEMS

Small animal experiments, especially with mice and rats, provide valuable information in the development of new drugs. Mice in particular seem to be the favored research animal because they share a large number of human genes and their colonies are relatively inexpensive to maintain compared with larger animals. In recent years, more than 90% of the animals used to understand mammalian biology were mice. The need for imaging small animals with a variety of modalities has been recognized by the health science community and small animal imaging systems have been developed for CT, ultrasound and MRI as well as PET. The value of small animal imaging has been recognized by the National Institutes of Health which has directed significant resources to funding instrument development and applications.[1, 2, 65-68]

Because of the high sensitivity associated with the radiotracers and their ability to deliver crucial information about physiological function, it is natural that PET is a major player in small animal imaging. Often the investigation of a new drug requires regional bio-distribution information at serial time points. Invasive techniques such as autoradiography provide high-resolution im-

ages of these distributions, but require long imaging times and, more importantly, a large number of animals. Because it is desirable to image the same animal over many serial time samples rather than sacrificing one or more animals for each time sample, the motivation to develop animal imaging is strong.

A. Estimated Scanner Requirements

Small animal PET imaging presents many challenges because of the small volumes that have to be imaged accurately. Table 5 contains a comparison of the parameters involved in human, rat, and mouse imaging. In a human scanner, the reconstructed spatial resolution is approximately 10 mm. To achieve similar sampling of the anatomy of the rat and mouse, the spatial resolution would have to be 1.7 and 0.75 mm respectively. Spatial resolution is not the sole factor in determining image quality. Because of statistical fluctuations, the count density in the resolution elements has to be matched if comparable image quality is desired. Comparisons of the associated resolution volumes alone suggests that the sensitivity of a scanner that could yield images at a 0.75 mm scale needs to be more than 2000 higher than a human scanner. This is clearly out of reach, but small size has one big advantage. In humans, attenuation reduces the coincidence event rate by more than a factor of 50. In the rat and mouse, the attenuation reduction is less than a factor of two. When attenuation is also considered, the required sensitivity increase is 5 at the rat level and 55 at the mouse level. These values while not as extreme are still formidable. To some degree, they can be mitigated by increasing the amount of activity administered to the animals. That also has constraints associated with the count rate capability of the scanner and the amount of injectate tolerated by the animal.[66]

Table 5. Imaging Scaling Comparison for Human and Small Animals

	Human	Rat	Mouse
Mass(g)	70,000	300	30
Blood volume (ml)	6000	25	2.5
cross section(cm^2)	700	20	4
Scaled resolution (mm)	10	1.7	0.75
Relative required sensitivity	1	200	2400
Attenuation factor	60	1.6	1.25
Rescaled sensitivity	1	5	55

B. Other Challenges

In addition to the imaging requirements, the small size of the mouse presents other challenges. One of the advantages of radiotracers in humans is that the amount of material administered is far too small to have any perturbing or toxic effects. For mice, this is not the case. The specific activity of the radiotracers as they are compounded for human studies is too low for mouse studies. High specific activities are required to reduce both the mass of the radiotracer and the volume of the injectate. The maximum volume that can be administered is about 10% of the blood volume, which is about 250 μl for a mouse. Anesthesia, sterility, and temperature control are additional concerns.

C. Design of Small Animal PET Systems

A number of small animal PET systems have been described in the literature and several are commercially available. These

designs seek to meet the requirements described above with the constraints of available technology and cost. Cost is not reduced in proportion to the size of the scanner since the number of detectors and corresponding electronics are comparable to human scanners. Commercial small animal PET systems Range in price from $500,000 to $1,000,000.

The Concorde Microsystems small animal PET scanner is based on the instrument designed at UCLA by Cherry et al. It uses 8 × 8 detector blocks of LSO crystals that are 2 × 2 × 10 mm. Thinner crystals are used to decrease the depth of interaction error, which is a bigger problem for small ring diameters. The output of each detector is transmitted to a 64-channel position sensitive photomultiplier tube. The detector rings have been arranged in two different configurations that are optimized for different sized animals. The P4 model has a ring diameter of 27 cm and can accommodate brain studies of small primates. The R4 model has a ring diameter of 15 cm and can image rats and mice. Both scanners have a spatial resolution of 1.8 mm at the center. This meets the spatial resolution requirements for rats, but falls short of the desired resolution for mice. The count sensitivities of these devices are matched reasonably well to the spatial resolution they can deliver. The newest small animal PET scanner available from Concorde is called the Focus®. It is similar in design to the R4, but uses 1 × 1 × 10 mm LSO crystals. This improves the spatial resolution to approximately 1.3 mm. This 30% improvement is substantial and results in significantly better image quality, but again is still far short of the submillimeter goal.

The other commercial system is the Philips Mosaic®, which is a scaled down version of the Philips Allegro whole body PET scanner. 16,680 individual 2 × 2 × 10 mm GSO crystals are assembled into a complete cylinder with an axial extent of 13 cm. An array of photomultipliers around the cylinder is used to determine the detectors involved in the coincidence event. This device has a spatial resolution of 2.2 mm and comparable sensitivity to the R4. Pictures of the R4 and Mosaic scanners are shown in Figure 45.[66, 69-71]

Figure 45. Commercial Small Animal PET Systems.

Concord μPET **Philips Mosaic**

E. Image Reconstruction

Image reconstruction for data acquired on the small animal scanner is very similar to that performed on the human scanners. The acquired projection data have to be corrected for random coincidences, attenuation, uniformity, and scatter. Because of the scanner geometry, all of these corrections except attenuation are as crucial to good image quality on the animal studies as they are on human studies. 3D reconstruction is performed using either Fourier rebinning or fully 3D iterative algorithms. Typical images are shown in Figure 46. These images demonstrate the adequacy of the systems for imaging rat anatomy and the potential for further improvement in mouse imaging.[47, 66, 72]

Figure 46. Rat and Mouse Images from a Small Animal PET System.

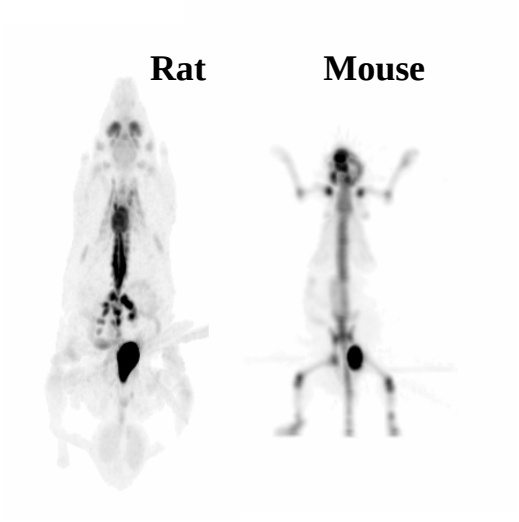

IX. FUTURE DEVELOPMENTS OF PET IMAGING

A. Applications

It is likely that the application of PET will branch out beyond diagnosis and staging. One example of this is the use of PET in radiation therapy treatment planning. PET provides a clearer picture of the metabolically active tumor tissue than MRI or CT. The integration of PET images into treatment planning is already a component in some commercial systems. Early evaluations suggest that PET significantly alters treatment planning. One report estimates that tumor volume delineation was altered in over 50% of cases and that this resulted in changed portal field sizes in more than 45% of patients. So far it is too early to demonstrate the efficacy of PET based on treatment outcome, but it seems likely that the role of PET in radiation therapy will continue to grow.[73, 74]

B. Detectors

The search for new and improved scintillators will continue. Of particular importance will be fast detectors. Current detector materials used in commercial PET systems are an order of magnitude too slow to provide useful time of flight information. Time of flight refers to capability of determining the position of a source based on the differential arrival times of the annihilation photons in a coincidence event. Fast scintillators do currently exist, but they do not have high enough stopping power for the required count sensitivity of PET systems. However, new scintillators with high density and atomic number as well as a scintillation decay time less than 1 nanosecond are actively being investigated.

C. Spatial Resolution and Count Sensitivity

The spatial resolution of current systems will be improved by using smaller detectors. Small animal PET systems are dealing with the problems of pushing the resolution envelope. Their success will be translated into improved human scanners. Although the search will continue for detectors with higher intrinsic efficiency, it is clear that bigger gains in sensitivity will come from increasing the axial coverage of the scanner. Future PET systems will have significantly larger axial field of view.

D. Computer Improvements

PET will also be affected positively by improvements in computer hardware and reconstruction algorithms. As the speed of the next generation of computer increases, higher dimension images will be used to preserve the full resolution of the scanner. Improvements in reconstruction algorithms will make them faster and will incorporate constraints more effectively producing enhanced image quality.

E. CT Improvements

As CT continues to evolve, the latest developments will be added to the PET/CT devices. In addition, the use of IV contrast in conjunction with PET/CT will continue to

increase to make the PET/CT the one stop shop for cancer evaluation.

F. Radiopharmaceuticals

Finally, it should be noted that new and better radiopharmaceuticals will be developed and commercialized. This is a necessity for the field to continue. Regardless of how much the instrumentation improves, the ultimate diagnostic information comes from the radiopharmaceutical. While F-18 FDG currently enjoys the role as the best cancer-imaging agent, it can be expected that progress in other diagnostic modalities will provide increasing competition. Fortunately, the potential for radiolabeling useful compounds is unlimited and the future of PET seems secure.

REFERENCES

1. Fowler, J. S., Volkow, N. D., Wang, G. J., Ding, Y. S., and Dewey, S. L., PET and drug research and development, *J Nucl Med* 40 (7), 1154-63, 1999.

2. MacLaren, D. C., Toyokuni, T., Cherry, S. R., Barrio, J. R., Phelps, M. E., Herschman, H. R., and Gambhir, S. S., PET imaging of transgene expression, *Biol Psychiatry* 48 (5), 337-48, 2000.

3. Arulampalam, T. H., Costa, D. C., Bomanji, J. B., and Ell, P. J., The clinical application of positron emission tomography to colorectal cancer management, *Q J Nucl Med* 45 (3), 215-30, 2001.

4. Bomanji, J. B., Costa, D. C., and Ell, P. J., Clinical role of positron emission tomography in oncology, *Lancet Oncol* 2 (3), 157-64, 2001.

5. Bombardieri, E. and Crippa, F., PET imaging in breast cancer, *Q J Nucl Med* 45 (3), 245-56, 2001.

6. Coleman, R. E., PET in lung cancer staging, *Q J Nucl Med* 45 (3), 231-4, 2001.

7. Delbeke, D. and Martin, W. H., Positron emission tomography imaging in oncology, *Radiol Clin North Am* 39 (5), 883-917, 2001.

8. Lewis, J. S. and Welch, M. J., PET imaging of hypoxia, *Q J Nucl Med* 45 (2), 183-8, 2001.

9. Giorgetti, A., Volterrani, D., and Mariani, G., Clinical oncological applications of Positron Emission Tomography (PET) using fluorine-18-fluoro-2-deoxy-D-glucose, *Radiol Med (Torino)* 103 (4), 293-318, 2002.

10. Shon, I. H., O'Doherty M, J., and Maisey, M. N., Positron emission tomography in lung cancer, *Semin Nucl Med* 32 (4), 240-71, 2002.

11. Becherer, A., Jaeger, U., Szabo, M., and Kletter, K., Prognostic value of FDG-PET in malignant lymphoma, *Q J Nucl Med* 47 (1), 14-21, 2003.

12. Fowler, J. S., Ding, Y. S., and Volkow, N. D., Radiotracers for positron emission tomography imaging, *Semin Nucl Med* 33 (1), 14-27, 2003.

13. Parsey, R. V. and Mann, J. J., Applications of positron emission tomography in psychiatry, *Semin Nucl Med* 33 (2), 129-35, 2003.

14. Rollo, F. D., Molecular imaging: an overview and clinical applications, *Radiol Manage* 25 (3), 28-32; quiz 33-5, 2003.

15. Medicare coverage issue manual transmittal 171, Centers for Medicare and Medicaid Services, 2003.

16. Budinger, T. F., PET instrumentation: what are the limits?, *Semin Nucl Med* 28 (3), 247-67, 1998.

17. Phelps, M. E. and Cherry, S. R., The Changing Design of Positron Imaging Systems, *Clin Positron Imaging* 1 (1), 31-45, 1998.

18. Fahey, F. H., Positron emission tomography instrumentation, *Radiol Clin North Am* 39 (5), 919-29, 2001.

19. Turkington, T. G. and Coleman, R. E., Clinical oncologic positron emission tomography: an introduction, *Semin Roentgenol* 37 (2), 102-9, 2002.

20. Nutt, R., The history of positron emission tomography, *Molecular Imaging and Biology* 4 (1), 11-26, 2001.

21. Blokland, J. A., Trindev, P., Stokkel, M. P., and Pauwels, E. K., Positron emission tomography: a technical introduction for clinicians, *Eur J Radiol* 44 (1), 70-5., 2002.

22. Muehllehner, G., Karp, J. S., and Surti, S., Design considerations for PET scanners, *Q J Nucl Med* 46 (1), 16-23, 2002.

23. Daube-Witherspoon, M. E., Zubal, I. G., and Karp, J. S., Developments in instrumentation for emission computed tomography, *Semin Nucl Med* 33 (1), 28-41, 2003.

24. Tarantola, G., Zito, F., and Gerundini, P., PET Instrumentation and Reconstruction Algorithms in Whole-Body Applications, *J Nucl Med* 44 (5), 756-69, 2003.

25. Karp, J. S., Against: Is LSO the future of PET?, *Eur J Nucl Med Mol Imaging* 29 (11), 1525-8, 2002.

26. Boellaard, R., Buijs, F., de Jong, H. W., Lenox, M., Gremillion, T., and Lammertsma, A. A., Characterization of a single LSO crystal layer high resolution research tomograph, *Phys Med Biol* 48 (4), 429-48, 2003.

27. Rafecas, M., Boning, G., Pichler, B. J., Lorenz, E., Schwaiger, M., and Ziegler, S. I., Inter-crystal scatter in a dual layer, high resolution LSO-APD positron emission tomograph, *Phys Med Biol* 48 (7), 821-48, 2003.

28. Muehllehner, G., Positron camera with extended counting rate capability, *J Nucl Med* 16 (7), 653-7, 1975.

29. Lewellen, T. K., Miyaoka, R. S., and Swan, W. L., PET imaging using dual-headed gamma cameras: an update, *Nucl Med Commun* 20 (1), 5-12, 1999.

30. Patton, J. A., Instrumentation for coincidence imaging with multihead scintillation cameras, *Semin Nucl Med* 30 (4), 239-54, 2000.

31. D'Asseler, Y., Vandenberghe, S., Winter, F. D., Van de Walle, R., Koole, M., Bouwens, L., Lemahieu, I., and Dierckx, R. A., PET imaging using gamma cameras, *Comput Med Imaging Graph* 25 (2), 87-96, 2001.

32. Grosev, D., Loncaric, S., Vandenberghe, S., and Dodig, D., Triple-head gamma camera PET: system overview and performance characteristics, *Nucl Med Commun* 23 (8), 809-14, 2002.

33. Adam, L. E., Karp, J. S., Daube-Witherspoon, M. E., and Smith, R. J., Performance of a whole-body PET

scanner using curve-plate NaI(Tl) detectors, *J Nucl Med* 42 (12), 1821-30, 2001.

34. Ollinger, J. M., Model-based scatter correction for fully 3D PET, *Phys Med Biol* 41 (1), 153-76, 1996.

35. Adam, L. E., Karp, J. S., and Freifelder, R., Energy-based scatter correction for 3-D PET scanners using NaI(T1) detectors, *IEEE Trans Med Imaging* 19 (5), 513-21, 2000.

36. Zaidi, H., Comparative evaluation of scatter correction techniques in 3D positron emission tomography, *Eur J Nucl Med* 27 (12), 1813-26, 2000.

37. Zaidi, H., Scatter modelling and correction strategies in fully 3-D PET, *Nucl Med Commun* 22 (11), 1181-4, 2001.

38. Werling, A., Bublitz, O., Doll, J., Adam, L. E., and Brix, G., Fast implementation of the single scatter simulation algorithm and its use in iterative image reconstruction of PET data, *Phys Med Biol* 47 (16), 2947-60, 2002.

39. Zaidi, H. and Hasegawa, B., Determination of the attenuation map in emission tomography, *J Nucl Med* 44 (2), 291-315, 2003.

40. Bedigian, M. P., Benard, F., Smith, R. J., Karp, J. S., and Alavi, A., Whole-body positron emission tomography for oncology imaging using singles transmission scanning with segmentation and ordered subsets-expectation maximization (OS-EM) reconstruction, *Eur J Nucl Med* 25 (6), 659-61, 1998.

41. Bendriem, B. E. and Townsend, D. W. E., *The Theory & Practice of 3d Pet*, 1st ed. Kluwer Academic Publishers, New York, 1998.

42. Defrise, M., Kinahan, P. E., Townsend, D. W., Michel, C., Sibomana, M., and Newport, D. F., Exact and approximate rebinning algorithms for 3-D PET data, *IEEE Trans Med Imaging* 16 (2), 145-58, 1997.

43. Matej, S., Karp, J. S., Lewitt, R. M., and Becher, A. J., Performance of the Fourier rebinning algorithm for PET with large acceptance angles, *Phys Med Biol* 43 (4), 787-95, 1998.

44. Liu, X., Defrise, M., Michel, C., Sibomana, M., Comtat, C., Kinahan, P., and Townsend, D., Exact rebinning methods for three-dimensional PET, *IEEE Trans Med Imaging* 18 (8), 657-64, 1999.

45. Mumcuoglu, E. U., Leahy, R. M., and Cherry, S. R., Bayesian reconstruction of PET images: methodology and performance analysis, *Phys Med Biol* 41 (9), 1777-807, 1996.

46. Qi, J. and Leahy, R. M., A theoretical study of the contrast recovery and variance of MAP reconstructions from PET data, *IEEE Trans Med Imaging* 18 (4), 293-305, 1999.

47. Chatziioannou, A., Qi, J., Moore, A., Annala, A., Nguyen, K., Leahy, R., and Cherry, S. R., Comparison of 3-D maximum a posteriori and filtered backprojection algorithms for high-resolution animal imaging with microPET, *IEEE Trans Med Imaging* 19 (5), 507-12, 2000.

48. Qi, J. and Leahy, R. M., Resolution and noise properties of MAP reconstruction for fully 3-D PET, *IEEE Trans Med Imaging* 19 (5), 493-506, 2000.

49. Townsend, D. W. and Beyer, T., A combined PET/CT scanner: the path to true image fusion, *Br J Radiol* 75 (Spec No), S24-30, 2002.

50. Bar-Shalom, R., Yefremov, N., Guralnik, L., Gaitini, D., Frenkel, A., Kuten, A., Altman, H., Keidar, Z., and Israel, O., Clinical performance of PET/CT in evaluation of cancer: additional value for diagnostic imaging and patient management, *J Nucl Med* 44 (8), 1200-9, 2003.

51. Cohade, C. and Wahl, R. L., Applications of positron emission tomography/computed tomography image fusion in clinical positron emission tomography-clinical use, interpretation methods, diagnostic improvements, *Semin Nucl Med* 33 (3), 228-37, 2003.

52. Fukui, M. B., Blodgett, T. M., and Meltzer, C. C., PET/CT imaging in recurrent head and neck cancer, *Semin Ultrasound CT MR* 24 (3), 157-63, 2003.

53. Schoder, H., Erdi, Y. E., Larson, S. M., and Yeung, H. W., PET/CT: a new imaging technology in nuclear medicine, *Eur J Nucl Med Mol Imaging* 5, 5, 2003.

54. Townsend, D. W., Beyer, T., and Blodgett, T. M., PET/CT scanners: a hardware approach to image fusion, *Semin Nucl Med* 33 (3), 193-204, 2003.

55. Beyer, T., Townsend, D. W., Brun, T., Kinahan, P. E., Charron, M., Roddy, R., Jerin, J., Young, J., Byars, L., and Nutt, R., A combined PET/CT scanner for clinical oncology, *J Nucl Med* 41 (8), 1369-79, 2000.

56. Kluetz, P. G., Meltzer, C. C., Villemagne, V. L., Kinahan, P. E., Chander, S., Martinelli, M. A., and Townsend, D. W., Combined PET/CT Imaging in Oncology. Impact on Patient Management, *Clin Positron Imaging* 3 (6), 223-230, 2000.

57. Picchio, M., Sironi, S., Messa, C., Mangili, G., Landoni, C., Gianolli, L., Zangheri, B., Vigano, R., Aletti Gde, M., De Cobelli, F., Del Maschio, A., Ferrari, A., and Fazio, F., Advanced ovarian carcinoma: usefulness of [(18)F]FDG-PET in combination with CT for lesion detection after primary treatment, *Q J Nucl Med* 47 (2), 77-84, 2000.

58. Beyer, T., Townsend, D. W., and Blodgett, T. M., Dual-modality PET/CT tomography for clinical oncology, *Q J Nucl Med* 46 (1), 24-34, 2002.

59. D'Amico, T. A., Wong, T. Z., Harpole, D. H., Brown, S. D., and Coleman, R. E., Impact of computed tomography-positron emission tomography fusion in staging patients with thoracic malignancies, *Ann Thorac Surg* 74 (1), 160-3; discussion 163, 2002.

60. Faber, T. L. and Garcia, E., Multimodality imaging, *Semin Nucl Med* 33 (3), 164-5, 2003.

61. Hutton, B. F. and Braun, M., Software for image registration: algorithms, accuracy, efficacy, *Semin Nucl Med* 33 (3), 180-92, 2003.

62. Stokking, R., Zubal, I. G., and Viergever, M. A., Display of fused images: methods, interpretation, and diagnostic improvements, *Semin Nucl Med* 33 (3), 219-27, 2003.

63. Goerres, G. W., Kamel, E., Heidelberg, T. N., Schwitter, M. R., Burger, C., and von Schulthess, G. K., PET-CT image co-registration in the thorax: influence of respiration, *Eur J Nucl Med Mol Imaging* 29 (3), 351-60, 2002.

64. Beyer, T., Antoch, G., Blodgett, T., Freudenberg, L. F., Akhurst, T., and Mueller, S., Dual-modality PET/CT imaging: the effect of respiratory motion on combined image quality in clinical oncology, *Eur J Nucl Med Mol Imaging* 30 (4), 588-96, 2003.

65. Cherry, S. R. and Gambhir, S. S., Use of positron emission tomography in animal research, *Ilar J* 42 (3), 219-32, 2001.

66. Chatziioannou, A. F., Molecular imaging of small animals with dedicated PET tomographs, *Eur J Nucl Med Mol Imaging* 29 (1), 98-114, 2002.

67. Schafers, K. P., Imaging small animals with positron emission tomography, *Nuklearmedizin* 42 (3), 86-9, 2003.

68. Phelps, M. E., PET: the merging of biology and imaging into molecular imaging, *J Nucl Med* 41 (4), 661-81, 2000.

69. Del Guerra, A. and Belcari, N., Advances in animal PET scanners, *Q J Nucl Med* 46 (1), 35-47, 2002.

70. Knoess, C., Siegel, S., Smith, A., Newport, D., Richerzhagen, N., Winkeler, A., Jacobs, A., Goble, R. N., Graf, R., Wienhard, K., and Heiss, W. D., Performance evaluation of the microPET R4 PET scanner for rodents, *Eur J Nucl Med Mol Imaging* 30 (5), 737-47, 2003.

71. Tai, Y. C., Chatziioannou, A. F., Yang, Y., Silverman, R. W., Meadors, K., Siegel, S., Newport, D. F., Stickel, J. R., and Cherry, S. R., MicroPET II: design, development and initial performance of an improved microPET scanner for small-animal imaging, *Phys Med Biol* 48 (11), 1519-37, 2003.

72. Qi, J., Leahy, R. M., Cherry, S. R., Chatziioannou, A., and Farquhar, T. H., High-resolution 3D Bayesian image reconstruction using the microPET small-animal scanner, *Phys Med Biol* 43 (4), 1001-13, 1998.

73. Ciernik, I. F., Dizendorf, E., Baumert, B. G., Reiner, B., Burger, C., Davis, J. B., Lutolf, U. M., Steinert, H. C., and Von Schulthess, G. K., Radiation treatment planning with an integrated positron emission and computer tomography (PET/CT): a feasibility study, *Int J Radiat Oncol Biol Phys* 57 (3), 853-63, 2003.

74. Paulino, A. C., Thorstad, W. L., and Fox, T., Role of fusion in radiotherapy treatment planning, *Semin Nucl Med* 33 (3), 238-43, 2003.

QUESTIONS

1. Carrier free radiotracers typically have no _____.
   a. radiation burden
   b. chemical toxicity
   c. particulate emissions
   d. gamma ray emissions

2. With positron emission, a _____ is turned into a _____.
   a. proton, neutron
   b. neutron, proton
   c. positron, electron
   d. electron, positron

3. Coincidence detection is better than conventional detection because _____.
   a. intrinsic efficiency is improved.
   b. patient radiation dose is less.
   c. the spatial resolution and sensitivity are better.
   d. the instrumentation is cheaper.

4. Radionuclides that emit positrons always
   a. have more neutrons than protons.
   b. have more protons than neutrons.
   c. have short half lives.
   d. yield annihilation radiation.

5. Which of the following is produced by a radionuclide generator?
   a. Oxygen-15
   b. Carbon-11
   c. Rubidium-82
   d. Fluorine-18

6. Annihilation radiation can be used with coincidence detection because _____.
   a. the energy is 511 keV.
   b. two photons are emitted.
   c. the photons are co-linear.
   d. it is easily absorbed.

7. For annihilation radiation, photoelectric absorption in tissue is _____.
   a. the only interaction.
   b. the most likely interaction.
   c. as likely as Compton scatter.
   d. very unlikely.

8. For annihilation radiation, photoelectric absorption depends primarily on the detector _____.
   a. temperature
   b. atomic number
   c. density
   d. proton to neutron ratio

9. Singles detectors require _____ for spatial resolution.
   a. geometric efficiency
   b. intrinsic efficiency
   c. good timing
   d. collimation

10. Coincidence detection requires at least ____ opposed detectors.
    a. 2
    b. 3
    c. 4
    d. 8

11. Random coincidences depend on
    a. the source activity.
    b. the detector geometric efficiency.
    c. the coincidence time window.
    d. all of the above.

12. Scattered radiation originating in the patient can be rejected because scattered photons have _____ compared to primary photons.
    a. higher energy
    b. lower energy
    c. different time characteristics
    d. different transmission

13. Whole body PET systems typically have between _____ and _____ individual detectors arranged in a cylinder.
    a. 90 and 180
    b. 900 and 1800
    c. 9000 and 18,000
    d. 90,000 and 180,000

14. The sampling rays defined by detector coincidence pairs are called _____.
    a. ray paths
    b. projections
    c. lines of response
    d. bins

15. The detector with the best intrinsic efficiency is _____
    a. BGO
    b. LSO
    c. GSO
    d. NaI(Tl)

16. The detector with the longest decay time is _____
    a. BGO
    b. LSO
    c. GSO
    d. NaI(Tl)

17. The detector that is radioactive is ____.
    a. BGO
    b. LSO
    c. GSO
    d. NaI(Tl)

18. The PET system with the best spatial resolution is the _____.
    a. HRRT
    b. Accel
    c. Allegro
    d. Advance

19. The most important factor affecting spatial resolution in a whole body PET system is _____.
    a. detector face size
    b. ring diameter
    c. detector thickness
    d. positron range

20. SPECT/PET systems have nearly the same _____ as dedicated PET systems.
    a. intrinsic spatial resolution
    b. sensitivity
    c. count rate capability
    d. NEC

21. One dedicated PET systems that uses scintillation camera technology is the _____.
    a. HRRT
    b. C-PET
    c. Accel
    d. Advance

22. The hot lung and skin artifacts are removed by _____ correction.
    a. sensitivity
    b. randoms
    c. scatter
    d. attenuation

23. The magnitude of the attenuation correction depends on _____.
    a. breconstruction algorithm
    b. path length from the source to the nearest detector
    c. total path length of both annihilation photons through the body
    d. path length from the source to the most distant detector

24. The process where cross plain data is accurately converted to direct plain data is called ____.
    a. backprojection
    b. filtered backprojection
    c. Fourier rebinning
    d. ordered subsets

25. One 3D iterative approach that is in current use is called _____.
    a. Fourier rebinning
    b. backprojection

c. filtered backprojection
d. RAMLA

26. The ____ allows meaningful comparisons of system sensitivity.
    a. NEC
    b. OS-EM
    c. RAMLA
    d. ML-EM

27. The true system sensitivity of 3D PET is approximately _____ times better than 2D PET.
    a. 2
    b. 4
    c. 8
    d. 16

28. In the design of 3D PET systems, the _____ are removed.
    a. lead septae between detector rings
    b. block detectors
    c. coincidence events
    d. count rate losses

29. Multislice CT is advantageous for PET/CT since there are fewer problems with _____.
    a. patient dose
    b. randoms correction
    c. scatter correction
    d. x-ray tube heat loading

30. The effective dose from a CT transmission study in PET/CT is about _____ mrem.
    a. 13
    b. 130
    c. 1300
    d. 13,000

31. The effective dose from a F-18 FDG study is about _____ mrem.
    a. 10,000
    b. 1000
    c. 100
    d. 10

32. Physicians reading head and neck PET/CT studies have to be especially aware of _____ artifacts.
    a. breathing
    b. metal
    c. truncation
    d. cross talk

33. Small animal PET scanners typically use detectors that are _____ compared to whole body PET systems.
    a. thicker
    b. thinner
    c. denser
    d. flatter

34. The future of PET most depends on new _____.
    a. instrumentation
    b. corrections
    c. reconstruction algorithms
    d. radiopharmaceuticals

35. Future PET scanners are likely to have larger _____.
    a. axial fields of view
    b. detector face size
    c. ring diameters
    d. count rate losses